Role of NLRP3-ASC inflammasomes on Glial Activation after mild Traumatic Brain Injury

Dissertation

zur Erlangung des Doktorgrades (Dr. med.)

der Medizinischen Fakultät

der Rheinischen Friedrich-Wilhelms-Universität

Bonn

TAO LI

aus Chengdu, China

2025

Angefertigt mit der Genehmigung
der Medizinischen Fakultät der Universität Bonn

1. Gutachter: Prof. Dr. med. Michael T. Heneka
2. Gutachter: Prof. Dr. Dirk Dietrich

Tag der Mündlichen Prüfung: 25. 08. 2025

Aus der Klinik und Poliklinik für Neurologie

Table of content

List of abbreviations

AD	Alzheimer's disease
ANOVA	Analysis of variance
AIM2	Absent in melanoma 2
APP	Amyloid precursor protein
ASC	Apoptosis-associated speck-like protein containing a C- terminal caspase recruitment domain
ATP	Adenosine triphosphate
BBB	Bood–brain barrier
BCA	Bicinchoninic acid
BSA	Bovine serum albumin
CCI	Controlled cortical impact
CHI	Closed head injury
CNS	Central nervous system
CSI	Controlled skull impact
CSF	Cerebrospinal fluid
DNA	Deoxyribonucleic acid
DAMPs	Damage-associated molecular pattern
DAPI	4',6-diamidino-2-phenylindole, dihydrochloride
dpi	Days post-injury
ELISA	Enzyme-linked immunosorbent assay
FTD	Frontotemporal dementia
GCS	Glasgow coma scale
GFAP	Glial fibrillary acidic protein
Iba1	Ionized calcium-binding adapter molecule 1
IFN	Interferon
IL	Interleukin
iNOS	Inducible nitric oxide synthase
KO	Knock out
LPS	Lipopolysaccharide
mTBI	mild Traumatic Brain Injury

MHC-II	Major histocompatibility complex class II
MRI	Magnetic resonance imaging
NF-κB	Nuclear factor kappa B
NFTs	Neurofibrillary tangles
NLRP3	Nucleotide-binding domain, leucine-rich repeat, and pyrin domain-containing protein 3
NLRs	Nucleotide-binding and oligomerization domain-like receptors
PAMPs	Pathogen-activated molecular patterns
PBS	Phosphate-buffered saline
PBST	PBS with Triton X-100
PFA	Paraformaldehyde
PRRs	Pattern recognition receptors
RIPA	Radioimmunoprecipitation assay
R-NSS	Revised Neurobehavioral Severity Scale
ROS	Reactive oxygen species
SEM	Standard error of the mean
TBI	Traumatic brain injury
TBST	Tris-buffered saline with Tween-20
TGF-β	Transforming growth factor-beta
TLRs	Toll-like receptors
TNF	Tumor necrosis factor
WB	Western blotting
WT	Wild type

1. Introduction

Traumatic brain injury (TBI) is an umbrella term that covers acquired acute brain insults resulting from a sudden external mechanical force to the head (Menon et al., 2010). It is currently one of the leading causes of death and permanent disability worldwide. Annually, nearly 69 million individuals worldwide endure TBI, with a particular impact in Europe and North America, resulting in a significant global social and economic burden (Dewan et al., 2018). Clinically, TBI severity is classified into three categories—mild, moderate, and severe—based on the Glasgow Coma Scale, post-traumatic amnesia, and loss of consciousness (Hart et al., 2016; Leo and McCrea 2016). Mild TBI (mTBI), also known as concussion, accounts for approximately 70 %–90 % of head injuries and is commonly caused by falls (Cassidy et al., 2004). Most individuals recover quickly from mTBI without significant cognitive deficits or visible brain changes on imaging. However, a subset of mTBI cases (10 %–15 %) experience persistent post-concussive symptoms, leading to a reduced quality of life, neurological dysfunction, and an increased risk of neuropsychiatric disorders such as depression and anxiety (Ahman et al., 2013; Rathbone et al., 2015). The term “hidden epidemic” is commonly associated with mTBI due to its widespread occurrence and the potential for impairments to worsen without prior indications (DePalma et al., 2015; Guskiewicz and Broglio, 2015; Powell et al., 2021). In recent years, several studies have shown that mTBI is an important non-age-related risk factor for the progression of neurodegenerative diseases, including Alzheimer’s disease (AD), Parkinson's disease (PD), and chronic traumatic encephalopathy (CTE) (Clark et al., 2022; Gardner et al., 2018; McKee et al., 2009). The neurological damage caused by mTBI is frequently heterogeneous, insidious, and persistent. However, our understanding of the fundamental pathophysiology of mTBI is limited, which presents obstacles in achieving early clinical diagnosis and timely intervention.

The pathophysiological course of TBI is commonly characterized by two distinct phases: primary injury and secondary damage. Primary injury is marked by immediate and direct damage resulting from mechanical forces, leading to structural destruction, ischemic edema, and cellular death. Subsequently, the secondary injury phase ensues, causing additional harm through persistent neuroinflamatory responses, oxidative activation, and neuroinflammatory response and contributes to the development of post-traumatic disorders. In recent years, advanced clinical imaging techniques have progressively

facilitated the *in vivo* visualization of glial reactivity, e.g., positron emission tomography tracers targeting the microglia-associated 18 kDa translocator protein (TSPO) (Van Camp et al., 2021). Furthermore, in individuals with mTBI, neuroinflammation has been observed to persist for up to 4 months, as indicated by significantly higher TSPO binding than that in healthy controls (Ebert et al., 2019). The activation of glial cells in mTBI not only leads to sustained glial inflammation but also impairs their capacity to efficiently phagocytose cellular debris. This dual effect results in several detrimental consequences, including neuronal damage, compromised synaptic plasticity, and the accumulation of abnormal protein aggregates (Johnson et al., 2012). Evidently, glial cells exhibit a propensity to release sustained and substantial levels of interleukin (IL)-1β following both isolated and repeated instances of mTBI. This cytokine has emerged as a critical pathogenic factor associated with the onset of neurological deficits and the progression of neurodegenerative diseases following head injury (Lv et al., 2022; Perez-Polo et al., 2013; Weil et al., 2014).

Concurrently, the nucleotide-binding domain, leucine-rich repeat, and pyrin domain-containing protein 3 (NLRP3) inflammasome has received increasing attention as a crucial constituent of the innate immune system, governing essential regulatory functions within the inflammatory cascade (Davis et al., 2011; Schroder and Tschopp, 2010). This multiprotein complex comprises three essential constituents: NOD-like receptor family, pyrin domain-containing 3 (NLRP3), apoptosis-associated speck-like protein containing a caspase recruitment domain (ASC), and pro-caspase-1 (pro-CASP-1). Innate immune cells, notably microglia and astrocytes, predominantly host this inflammasome complex. Upon activation, this inflammasome stimulates glial cells to process and release cytokines such as IL-1β and IL-18, concomitantly promoting cell pyroptosis (Franchi et al., 2009; Jha et al., 2010). In addition, the significance of the NLRP3 inflammasome in both TBI and neurodegenerative conditions has attracted substantial research attention (Halle et al., 2008; Heneka et al., 2013; Xu et al., 2018). Multiple experiments have confirmed that following moderate or severe TBI, the NLRP3 inflammasome not only triggers a robust inflammatory response glial cell, resulting in secondary neurological damage (Dempsey et al., 2017; Liu et al., 2013; Xu et al. 2018), but also can provide insights into the prognosis of patients during their post-traumatic recovery (Kerr et al., 2018). However, comprehensive validation of its role in mTBI progression remains incomplete. Given the

sustained release of cytokines, especially IL-1β, resulting from glial activation after mTBI, we posit a plausible connection between prolonged glial inflammation and NLRP3 activation following mTBI. To enhance clarity, the following paragraphs delve into the characteristics of microglia and astrocytes in the central nervous system (CNS) and their roles in glial-mediated inflammatory processes. Subsequently, we shift our focus to explore the inflammatory response of and morphological changes in glial cells in the context of mTBI, particularly emphasizing the impact of NLRP3 inflammasome activation on the glial inflammatory response. Lastly, we outline the study objectives within the context of the current limitations in the field of research on mTBI and NLRP3.

1.1 Roles of Microglia and Astrocytes in the CNS

Glial cells, including microglia, astrocytes, oligodendrocytes, and ependymal cells, are critical for supporting and regulating neuronal function in the CNS. Microglia, as the resident immune cells of the CNS, possess a distinct origin from other glial cells, arising from myeloid progenitor cells in the yolk sac during embryonic development. In contrast, astrocytes are derived from neural stem cells that give rise to various progenitor cells during early brain development. Similarly, oligodendrocytes originate from neural stem cells or glial progenitor cells in the developing CNS, and ependymal cells emerge from the specialized neuroepithelium (Verkhratsky et al., 2019). Notably, microglia and astrocytes are the two main types of glial cells involved in maintaining physiological homeostasis and inducing pathological changes (Jha et al., 2019; Vainchtein and Molofsky, 2020).

1.1.1 Physiological Functions of Microglia and Astrocytes

In the CNS, Microglia are constantly active, serving as the brain's resident immune cells. They carefully monitor their surroundings, clear away cellular debris and damaged cells through a process called phagocytosis and help regulate immune responses to maintain a stable environment within the brain (Heneka et al., 2014). Besides their immune role, microglia are also involved in shaping the structure of neural networks. They remove weak or unnecessary synapses — the connections between nerve cells — through a process known as synaptic pruning. This function is particularly important during brain development, as it helps to refine neural circuits and supports proper brain function (Hong et al., 2016; Ghosh et al., 2018). Astrocytes, another major type of glial cell, usually remain

inactive under normal conditions. However, they contribute significantly to brain homeostasis. Astrocytes help maintain the blood-brain barrier (BBB), a protective structure that controls the movement of substances between the bloodstream and brain tissue (Liddelow and Barres, 2017; Wang and Parpura, 2016). Like microglia, astrocytes can also participate in synaptic pruning and immune responses, especially when the brain is under stress or injury. Furthermore, astrocytes play a vital role in regulating communication between neurons by controlling the uptake and recycling of neurotransmitters, such as glutamate, which is essential for proper neuronal signaling (Dejakaisaya et al., 2021; Li et al., 2021a). Notably, both microglia and astrocytes are equipped with pattern recognition receptors (PRRs), including Toll-like receptors (TLRs) and NOD-like receptors, which enable them to detect signals of tissue damage or infection. When these cells recognize such signals, called damage-associated molecular patterns (DAMPs) or pathogen-associated molecular patterns (PAMPs), they can quickly activate immune-related pathways and contribute to the brain's defense and repair mechanisms. This process is generally referred to as glial cell activation. (L. Li et al., 2021; Freeman et al., 2017; Garaschuk and Verkhratsky, 2019; Kumar, 2019; Rodríguez-Gómez et al., 2020).

1.1.2 Glial Inflammatory Response

Glial cells, especially microglia, play a central role in the brain's immune responses. They are highly adaptable and can exhibit a variety of functional states depending on the situation. In the past, microglia were often classified into two main types: M1 (pro-inflammatory) and M2 (anti-inflammatory), like the classification used for macrophages (Orita et al., 1986). However, this simple classification is now considered insufficient. Microglia display a wide range of states influenced by immune signals, their specific location within the brain, and environmental conditions (Paolicelli et al., 2022). These different activation patterns allow microglia to either help resolve inflammation or contribute to tissue damage, depending on the context. During infections or injury, microglia can release pro-inflammatory molecules, such as interleukin-1β (IL-1β), tumor necrosis factor-alpha (TNF-α), and inducible nitric oxide synthase. While these molecules are important for defending the brain against threats, excessive or prolonged release can lead to damage to neurons and glial cells. On the other hand, microglia also produce

protective factors, such as transforming growth factor-beta (TGF-β) and interleukin-10 (IL-10), which help to control inflammation and support tissue repair. Astrocytes, although traditionally seen as supportive cells, also participate in immune responses. When exposed to harmful stimuli like bacterial infections, they may release molecules that impair the brain's ability to form new connections (neuroplasticity) and contribute to further damage. However, in conditions like stroke, astrocytes can also switch to a protective role, working to restore balance and reduce injury (Zamanian et al., 2012). These dynamic and sometimes opposing actions of glial cells are crucial for determining whether inflammation in the brain resolves properly or becomes chronic and harmful.

1.2 Glia-mediated Neuroinflammation in Traumatic Brain Injury

Neuroinflammation, largely driven by activated glial cells, plays a key role in the progression and outcome of TBI. Following a brain injury, glial cells respond quickly, but the way they react over time can either help the brain recover or worsen the damage (Johnson et al., 2013; Roth et al., 2014).

1.2.1 Acute Inflammation after Trauma

Immediately after TBI, the environment within the brain changes dramatically. The injury often leads to reduced blood flow, lack of oxygen (hypoxia), and disruption of the BBB (Jin et al., 2012a). In response, microglia and astrocytes become activated and start releasing a variety of signaling molecules. These include pro-inflammatory cytokines, such as IL-1β and TNF-α, which help recruit immune cells and initiate repair processes but can also cause additional cell damage. At the same time, they also produce anti-inflammatory factors, like IL-4 and IL-10, which help limit inflammation and support tissue healing (Doğanyiğit et al., 2022; Jassam et al., 2017; Sordillo et al., 2016; Webster et al., 2017). Clinical studies have shown that the levels of pro-inflammatory cytokines such as IL-6, IL-1β, and IL-8 increase within the first few days after TBI. In contrast, anti-inflammatory cytokines like IL-10 show a delayed response, peaking around five days after the injury (Thelin et al., 2017; Zeiler et al., 2017). These opposing signals create a delicate balance: while inflammation is necessary to remove damaged cells and start repair, too much or uncontrolled inflammation may worsen the injury by causing further cell stress and death.

1.2.2 Sustained Inflammation after Traumatic Brain Injury

After the initial (acute) phase, inflammation often continues due to the release of DAMPs from injured cells (Heneka et al., 2014). These molecules keep glial cells, especially microglia, in an activated state and promote the production of harmful substances like reactive oxygen species (ROS). Excessive ROS can damage cell membranes, disrupt cellular energy production, leading to lipid peroxidation, adenosine triphosphate (ATP) release and, ultimately, cellular death (Russo and McGavern, 2015). TBI also causes a phenomenon known as "glial priming," where microglia become more sensitive and reactive, maintaining elevated levels of immune markers such as MHC class II. This means that even minor future stimuli can trigger an exaggerated inflammatory response (Fenn et al., 2014; Muccigrosso et al., 2016). Other stress markers, such as cluster of differentiation 68 and nicotinamide adenine dinucleotide phosphate oxidase 2, have been observed to be maintained at elevated levels for extended periods, even up to a year following head injury (Loane et al., 2014). This prolonged neuroinflammation can lead to a series of negative consequences, such as loss of synapses, damage to nerve fibers (axons), impaired glial function, and accumulation of abnormal proteins (Loane et al., 2014; Chen et al., 2017). These processes contribute to the accelerated progression of neurological deficits and neurodegenerative processes (Brett et al., 2022).

1.3 Morphological Alterations of Microglia and Astrocytes in Traumatic Brain Injury

Both microglia and astrocytes exhibit a wide range of functional activities and adaptive morphologies in response to environmental stimuli (Szabo and Gulya, 2013; Savage et al., 2019; Zhou et al., 2019).

1.3.1 Morphological Changes in Microglia

Prior to trauma, microglia, the resident immune cells of the CNS, exhibit a branched or "ramified" shape. This morphology allows them to constantly monitor the brain environment (Schlegelmilch et al., 2011). However, following injury, microglia rapidly change their appearance depending on the stage and severity of damage. In the acute and subacute phases, microglia often adopt shapes such as bipolar/rod-shaped, hypertrophic, or amoeboid forms (Sun et al., 2020; Yang et al., 2015; Ziebell et al., 2012). These activated forms are characterized by enlarged cell bodies and shortened or swollen

processes and visualized classically using ionized calcium-binding adapter molecule 1 (Iba1), a widely used microglial markers (González Ibanez et al., 2019). Each morphology is associated with distinct functions. For example, bipolar/rod-shaped microglia tend to proliferate during the early and recovery phases after injury (Tam and Ma, 2014; Ziebell et al., 2012). Hypertrophic microglia, often referred to as "primed" microglia, show reduced environmental surveillance but heightened sensitivity to inflammatory stimuli (DiBona et al., 2019; Walker and Lue, 2015). Amoeboid microglia are highly active in releasing pro-inflammatory molecules and in clearing cellular debris through phagocytosis (Crain et al., 2013; X. Liu et al., 2017). In the long-term (>21 days post-injury) or chronic phase of TBI, microglia often exhibit a less branched structure and an increase in inflammatory gene expression, which correlates with cognitive decline and behavioral deficits (Fenn et al., 2014; Muccigrosso et al., 2016). Interestingly, persistent stress or aging can trigger a "dystrophic" microglial morphology, characterized by fragmented processes and spherical swellings (Gorgoulis et al., 2019; Ritzel et al., 2018, 2019). Compared to hypertrophic microglia, dystrophic microglia tend to lose their protective roles and contribute more to chronic inflammation, which is linked to neurodegenerative diseases like Alzheimer's disease (Angelova and Brown, 2019; Streit et al., 2009). These findings highlight the diverse morphological states of microglia and their involvement in the pathological response to TBI.

1.3.2 Morphological Changes in Astrocytes

Similar to microglia, astrocytes undergo morphological changes closely tied to their functional shifts (Althammer et al., 2020; Liddelow and Barres, 2017). In homeostasis, protoplasmic astrocytes display short and primarily branched tertiary processes near neuronal synapses (Zhou et al., 2019). After an acute insult, activated astrocytes show upregulated glial fibrillary acidic protein (GFAP) expression and undergo hypertrophic responses, characterized by process elongation and cell body enlargement in the injured and surrounding areas (Robinson et al., 2016; Susarla et al., 2014). This reaction can be detected as early as 7 days after injury and may persist for several weeks, especially in mild to moderate TBI models (Susarla et al., 2014). While reactive astrocytes play a protective role by forming a physical barrier—known as a glial scar. The primary role of glial scarring is to build a physical barrier around the injured site, isolating it from healthy

tissue and curtailing damage propagation (Sofroniew et al., 2009). Nevertheless, this barrier can also hinder axonal regeneration and impede new neural connectivity, thus hampering functional recovery and contributing to prolonged impairments after CNS injury (Ribotta et al., 2004; Silver and Miller, 2004; Wanner et al., 2008).

1.3.3 Morphological Interaction Between Microglia and Astrocytes

Abundant research has highlighted a strong connection between morphological alterations in microglia and astrocytes following TBI (Morrison et al., 2017; Witcher et al., 2018). Specifically, during the initial phases, the appearance of rod-shaped microglia is often accompanied by astrocyte hypertrophy and increased GFAP expression (Witcher et al., 2018). Although these two glial types do not always directly contact each other immediately after injury (Taylor et al., 2014; Ziebell et al., 2012). In the following stages, increasing evidence suggests that cytokines and chemokines derived from microglia, including IL-1β and TNF-α, play a crucial role in inducing astrogliosis and aggregation after a CNS injury (Balasingam et al., 1994; Norris et al., 1994). Simultaneously, proliferating microglia engage in morphological interactions with astrocytes during the peak of glial inflammation. These interactions carry significant implications for the formation of glial scars (Sofroniew et al., 2009; Wang et al., 2018a). Furthermore, astrogliosis or components of glial scars may play a role in modulating the accumulation of additional microglia/macrophages, thereby amplifying the immune response to central damage (Hayashi et al., 2001; Haynes et al., 2006; Rhodes et al., 2003) Notably, astrocytes can participate directly in clearing damaged cells and debris through a process called phagocytosis, particularly when microglia become dysfunctional. Interestingly, astrocytes can also interact directly with dysfunctional microglia, using their processes to engulf apoptotic cells and clear microglial debris (Konishi et al., 2020). These complex interactions between microglia and astrocytes play a critical role in shaping theinflammatory and repair processes following brain injury.

1.4 NLRP3 Inflammasome Activation: A Key Role in Glial Inflammatory Cascades after Traumatic Brain Injury

In recent decades, the activation of the NLRP3 inflammasome in glial cells has been demonstrated to play a significant role in the cascade of neuroinflammatory processes after TBI (Irrera et al., 2020; O'Brien et al., 2020a). This activation is thought to occur via

two main steps in vitro models:

(1) Priming: Research has highlighted that specific DAMPs present in the cellular environment prime the NLRP3 inflammasome in glial cells, particularly microglia, via TLRs and nuclear factor kappa B (NF-κB) signaling (Halle et al., 2008; Swanson et al., 2019). These DAMPs include ROS, high-mobility group box 1, S100 proteins, extracellular matrix molecules, and heat shock protein (Braun et al., 2017; O'Brien et al., 2020b). The priming event leads to the transcriptional upregulation of critical NLRP3 inflammasome components, including the sensor molecule NLRP3, the adaptor protein ASC, and the effector protein pro-CASP 1 (Sutterwala et al., 2006). Indeed, it is crucial to underscore that the priming phase sensitizes the NLRP3 inflammasome, as NLRP3 itself does not demonstrate significant inflammatory activity at this stage.

(2) Activation: Activation of the NLRP3 inflammasome involves multiple pathways due to its broad range of ligands. It can be activated through various mechanisms, including 1) extracellular ATP, which induces K^+ efflux via the P2X7 receptor; 2) ROS, generated by DAMPs; 3) the formation of crystalline or granular structures within cells, resulting in lysosomal rupture and release of lysosomal contents such as cathepsin B; 4) endoplasmic reticulum stress; 5) autophagy dysfunction; and 6) Ca^{2+} overload (Gombault et al., 2012; Muñoz-Planillo et al., 2013; Swanson et al., 2019). These stimuli activate NLRP3, initiating the assembly of ASC and recruiting CASP-1, resulting in the formation of a functional NLRP3 inflammasome complex (Sutterwala et al., 2006). This complex then facilitates the activation of CASP-1 through proximity-induced interactions, leading to the maturation of IL-1β and IL-18. Moreover, the activation of the inflammasome can induce cell death directly through pyroptosis or indirectly through apoptosis (Franchi et al., 2009; Irrera et al., 2017; S. Jha et al., 2010; Shi et al., 2015; Xu et al., 2018). These research findings have significantly advanced our understanding of the pathological mechanisms driving glia-mediated neuroinflammation, particularly in the context of conditions such as brain trauma and neurodegeneration.

1.5 The Role and Impact of the NLRP3-ASC Inflammasome in Traumatic Brain Injury

Notably, several inflammasomes, such as the NLRP3, absent in melanoma 2 (AIM2), and NLRP1 inflammasomes, have been closely associated with TBI (de Rivero Vaccari et al., 2014; Freeman and Ting, 2016; Ge et al., 2018). Since the initial observation by Liu et al.

in 2013, there has been significant interest in understanding NLRP3 inflammasome in TBI, particularly in moderate and severe cases (Dempsey et al., 2017; Liu et al., 2013; Xu et al. 2018). They have reported an increase in the levels of NLRP3 inflammasome components (NLRP3, ASC, caspase-1, and IL-1β) within 24 hours after injury, with sustained upregulation observed for up to 3–7 days after controlled cortical impact in rat models. Clinical investigations have also demonstrated that, in children, cerebrospinal fluid NLRP3 levels exceeding 6.63 ng/mL following severe TBI were independently associated with a poor outcome at 6 months post-TBI, as determined using the Glasgow Outcome Scale (Wallisch et al., 2017). In preclinical models of TBI, treatment with specific inhibitors of NLRP3 (MCC950 and JC-124) has shown to reduce neuroinflammation, alleviate BBB damage, and mitigate apoptosis in TBI mouse models (Ismael et al., 2018; Kuwar et al., 2019). The NLRP3-deficient mouse model has demonstrated significant improvements in Revised Neurobehavioral Severity Scale (R-NSS) scores during the acute phase, as well as enhanced motor function and cognitive performance during the subacute phase (Ismael et al., 2018; Xu et al., 2018).

ASC is a common and crucial adapter for the inflammasome aggregation (e.g., NLRP3, AIM2, Pyrin). Some inflammasomes, like mouse NLRP1 and NLRP2 can bypass ASC and directly recruit caspase-1. However, the efficiency of cytokine maturation may be reduced without ASC (Guo et al., 2015; Van Opdenbosch et al., 2014). ASC could form aggregates called specks during its activation, promoting to cleavage of pro-caspase-1 and pro-IL-1 β and activating inflammatory response (Bryan et al., 2009). Clinically, serum levels of ASC exceeding 547.6 pg/mL exhibited a sensitivity of 85.71 % and specificity of 100 % in predicting poorer neurological outcomes following TBI in individuals aged over 20, as assessed using the Glasgow Outcome Scale-Extended (Kerr et al., 2018). In animal models, ASC inhibition has been shown to improve performance in tasks evaluating motor function, cognition, and behavior during TBI recovery (Wang et al., 2021).

The NLRP3-ASC inflammasome offers valuable insights into the potential connection between these two pathological processes. However, the mechanisms through which the inflammation triggered by the inflammasome transitions from the acute phase of TBI to the chronic phase, and subsequently contributes to neurodegenerative processes, remain unclear.

1.6 Knowledge Gap on NLRP3-ASC inflammasome in mild Traumatic Brain Injury

While research on the NRLP3-ASC inflammasome in the context of TBI has yielded valuable insights, a limited number of studies have directly confirmed the activation of the inflammasome and its potential impact on neuropathological outcomes after mTBI. Moreover, most studies have focused on the acute and subacute phases of injury, leaving the long-term consequences of NLRP3-ASC inflammasome activation in TBI insufficiently investigated (O'Brien et al., 2020; Wu et al., 2022). Comprehending the temporal evolution of inflammasome activation and its repercussions in persistent neuroinflammation is of paramount importance. This will address a substantial knowledge gap concerning the mechanisms that contribute to delayed neurological dysfunction and, potentially, the onset of neurodegenerative processes in individuals with mTBI. A more comprehensive understanding of these intricate mechanisms is essential for developing precise therapeutic strategies aimed at mitigating neurological impairment in individuals with mTBI.

1.7 Hypothesis

We hypothesized that sustained glial inflammation, driven by NLRP3-ASC inflammasome activation, contributes to the long-term effects following mild traumatic brain injury.

1.8 Aims

1.8.1 General Aims

To characterize the role of NLRP3-ASC inflammasome in glial cells following mTBI.

1.8.2 Specific Aims

1. Characterizing NLRP3-ASC Inflammasome-related Proteins Following mTBI: The first specific aim of this study was to comprehensively characterize NLRP3- ASC inflammasome in the context of mTBI.

2. Evaluating the Inflammatory Responses of Glial Cells: This aim was to assess inflammatory responses of microglia and astrocytes following the mTBI, shedding light on how glial inflammation contribute to the progression of mTBI.

3. Temporal Analysis of Inflammasome aggregation in Glial Cells: This aim involved a temporal analysis of ASC aggregation in glial cells to understand how ASC related-

inflammasome evolves over time post-mTBI.

4. Investigating Glial Morphology and Interactions Following mTBI: This aim focused on the morphological changes of microglia and astrocytes in the context of glial inflammation and explores how their interactions contribute to the overall response to mTBI.

5. Exploring Other Pathological Mechanisms: The final aim was to explore additional pathological pathway or inflammasome beyond NLRP3-ASC axis that may be involved in mTBI.

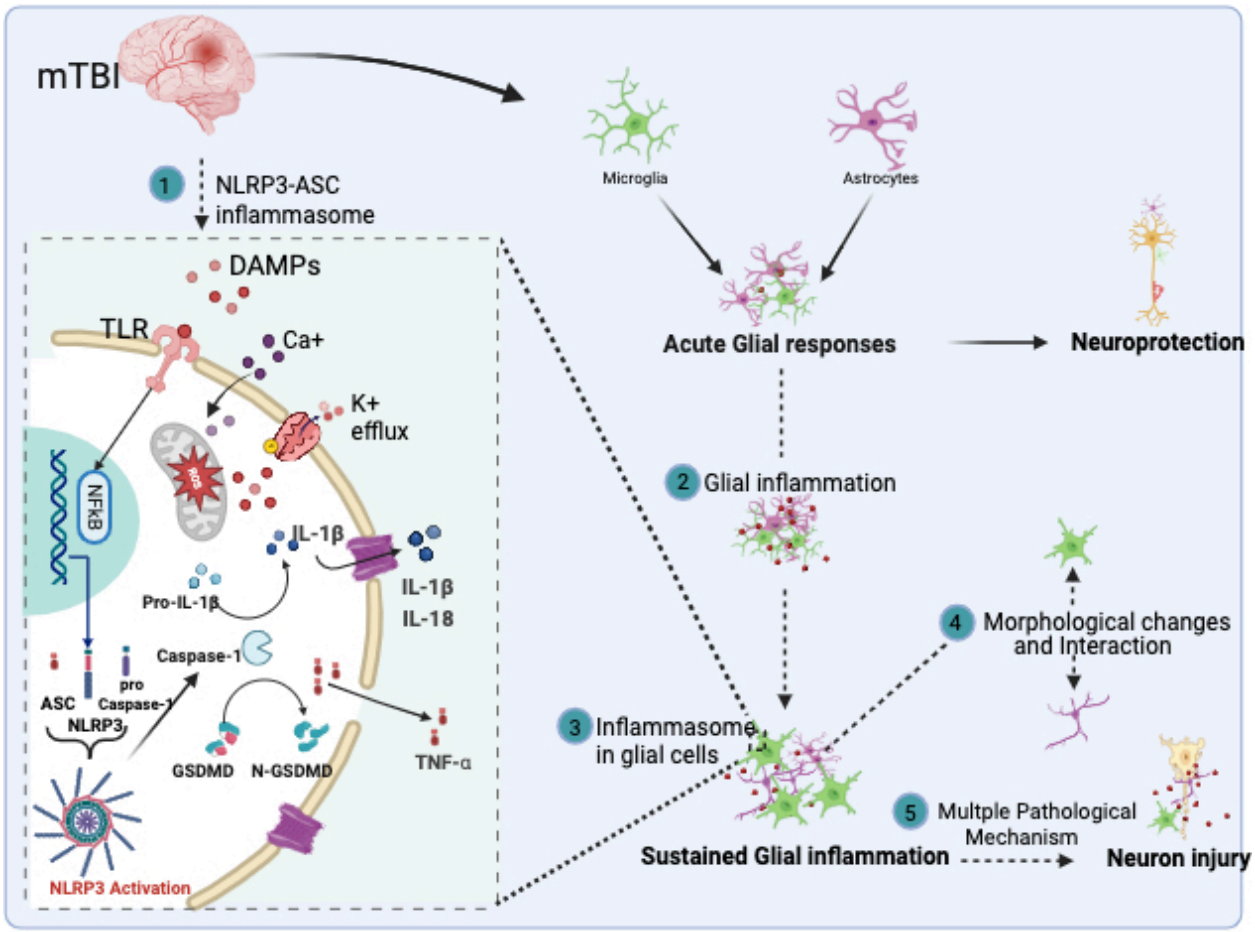

Fig. 1: The potential role of NLRP3-ASC inflammasome in sustained glial inflammation following mTBI

Schematically, the early phase of mTBI is characterized by an acute glial response, which potentially serves as a defense mechanism against damage. However, as time progresses, the glial cells undergo sustained inflammation, ultimately resulting in neurological dysfunction.

In this pathological process, we hypothesis that the NLRP3-ASC inflammasome is volved in the activation of glial cells following mTBI. In response to various DAMPs, NLRP3-ASC inflammasome within glial cells catalyzes the cleavage of CASP-1 and GSDMD, resulting in the maturation and release of cytokines such as IL-1β and TNF-α. Concurrently, glial cells undergo functional and morphological changes, interacting with each other in the context of inflammasome. These maladaptive glial responses promote the persistent glial inflammation, leading to neuron damage or deficit through a variety of pathological mechanisms. The dotted arrow in the figure symbolizes the research direction, indicating an exploration of the NLRP3 pathway's involvement in glial cell inflammatory responses in the context of mTBI. This investigation aligns with the outlined objectives 1, 2, 3, 4, and 5. Note: The figure was created using the Biorender website.

2. Materials and Methods

2.1 Materials

2.1.1 Antibodies

2.1.1.1 Tab. 1: Antibodies used for Immunohistochemistry

Antibody	Manufacture	Cat.no. (RRID)	Dilution
ASC	Cell Signaling (Frankfurt, Germany)	D2W8U #67824 Rabbit anti-Mouse	1:1000
Iba1	Abcam (Cambridge, UK)	ab289874 Goat anti-Mouse	1:1000
GFAP	Thermo Fisher (Waltham, USA)	2.2B10 Rat anti-Mouse	1:300
Iba1	Wako (Neuss, Germany)	01919741 Rabbit anti-Mouse	1:1000
Neun	Merck (Munich, Germany)	MAB377 Rabbit anti-Mouse	1:100
IL-1β	RD SYSTEMS (Minneapolis, USA)	AF-401-SP Goat anti-Mouse	1:500
Caspase 3	Cell Signaling (Frankfurt, Germany)	D3E9 #9579 Rabbit anti-Mouse	1:1000
P53	Abcam (Cambridge, UK)	ab131442 rabbit anti-mouse	1:500
Alexa Fluor 488	Invitrogen (Darmstadt, Germany)	A-11017 (AB_2534084), Goat anti-Rabbit	1:500
Alexa Fluor 594	Invitrogen (Darmstadt, Germany)	A-11032 (AB_2534091), Goat anti-rabbit	1:500
Alexa Fluor 647	Invitrogen (Darmstadt, Germany)	A-21247 (AB_141778), Goat anti-Rat	1:500
Alexa Fluor 488	Invitrogen (Darmstadt, Germany)	A-11006 (AB_2534074), Rat anti-Goat	1:500

Abbreviations: ASC, apoptosis-associated speck-like protein containing a C-terminal caspase recruitment domain; Iba1, allograft inflammatory factor 1; IL, interleukin; GFAP, glial fibrillary acidic protein.

2.1.1.2 Tab. 2: Antibodies used for Immunoblotting analysis

Antibody	Manufacture	Cat.no. (RRID)	Dilution
ASC	Cell Signaling (Frankfurt, Germany)	D2W8U #67824 Rabbit anti-Mouse	1:1000
IL-1β	Cell Signaling (Frankfurt, Germany)	E7V2A #63124 Rabbit anti-Mouse	1:1000
NLRP3	Cell Signaling (Frankfurt, Germany)	D4D8T #15101 Rabbit anti-Mouse	1:500
Caspase 1	ipoGen (UAS)	0 mAb (Casper-1) Rat anti-Mouse	1:1000
Caspase 3	Cell Signaling (Frankfurt, Germany)	D3E9 #9579 Rabbit anti-Mouse	1:1000
Caspase 8	Cell Signaling (Frankfurt, Germany)	D5B2 #14071 Rabbit anti-Mouse	1:1000
GAPDH	Cell Signaling (Frankfurt, Germany)	#2118 Rabbit anti-Mouse	1:20,000
IRDye 800CW	I-COR Biosciences (Lincoln, NE, USA)	926-32219 (AB_1850025) Goat anti-Rat	1:20,000
IRDye 680RD	I-COR Biosciences (Lincoln, NE, USA)	926-68072 (AB_10953628) Donkey anti-Rabbit	1:20,000

Abbreviations: ASC: apoptosis-associated speck-like protein containing a C-terminal caspase recruitment domain; IL: interleukin; NLRP3: nucleotide-binding domain, leucine rich repeat, and pyrin domain-containing protein 3; GAPDH: glycerinaldehyde-3 phosphate-dehydrogenase.

2.1.2 Buffers

Tab. 3*:* List of buffers

Buffer	Manufacture	Reagent	Dilution	Cat. no.
Immunohistochemistry				
PBST (pH 7.4)	Carl Roth (Karlsruhe, Germany)	Triton X-100	0.1 % (v/v)	3051.3
	Carl Roth (Karlsruhe, Germany)	PBS	0.01 M	L182-10
Citrate buffer (pH 6.0)	Carl Roth (Karlsruhe, Germany)	Trisodium citrate	100 M	3580.3

Buffer	Manufacture	Reagent	Dilution	Cat. no.
Block buffer	Abcam (Cambridge, UK)	Normal goat serum	10 % (v/v) NGS + PBST	ab7481
	Rockland Immunochemicals (Limerick, PA, USA)	BSA	3 % (v/v) BSA + PBST	BSA-500
Western blotting				
RIPA (pH 7.2)	(Eschwege, Germany)	SDS	3.5 mM	811030
	PanReac AppliChem (Darmstadt, Germany)	NaCl	75 mM	131659
	Carl Roth (Karlsruhe, Germany)	Tris	25 mM	5429.3
	US Biological (Swampscott, MA, USA)	NP-40	16 mM	N3500
	LI-COR Biosciences (Lincoln, NE, USA)	Na-DOC	12 mM	D6570
Homogenization buffer	Carl Roth (Karlsruhe, Germany)	EGTA	1 mM	6054.2
	Thermo Fisher (Waltham, USA)	Protease-Inhibitor-Cocktail	1:100	87785
	Carl Roth (Karlsruhe, Germany	NaF	5 mM	P756.1
	Sigma-Aldrich (Munich, Germany)	Pyrophosphate	20 mM	P8135
	Sigma-Aldrich (Munich, Germany)	AEBSF	1 mM	A8456
TBST (pH 7.5)	Carl Roth (Karlsruhe, Germany)	Tris	5 mM	5429.3
	PanReac AppliChem (Darmstadt, Germany)	NaCl	15 mM	131659
	Carl Roth (Karlsruhe, Germany)	Tween 20	0.01 % (v/v)	9127.1
Blocking buffer	Rockland Immunochemicals (Limerick, PA, USA)	BSA	3 % BSA + TBST	BSA-50

Buffer	Manufacture	Reagent	Dilution	Cat. no.
PFA	Sigma-Aldrich (Munich, Germany)	Paraformaldehyde solution	4 % in PBS	P6148
Sudan Black staining system	Sigma-Aldrich	Sudan Black b	0.01 % in Ethanol	199664
	(Munich, Germany)			
NuPAGE MOPS running buffer	Invitrogen (Darmstadt, Germany)	NuPAGE™ MOPS SDS Running Buffer (20X)	1× dilution in dd water	NP0001

Abbreviations: BSA: bovine serum albumin; PBS: phosphate-buffered saline; PBST: phosphate-buffered saline with Triton X-100; RIPA: radioimmunoprecipitation assay; TBST, Tris-buffered saline with Tween 20; PFA: paraformaldehyde.

2.1.3 Instruments and Consumables

Tab. 4: List of instruments and Consumables

Material	Manufacturer	Cat. No. (RRID)
Trauma injury construction and tissue collection		
Stereotaxic frame	Stoelting (Dublin, Ireland)	68037
Stereotaxic Impactor	Leica Biosystems (Germany)	655432
Insulin syringes	BD Medical (Le Pont-de-Claix, France)	324826
Immunohistochemistry		
Vibratome	Leica Biosystems (Wetzlar, Germany)	LEICA VT1000 S
SuperFrost microscope slides	LI-COR Biosciences (Lincoln, NE, USA)	12372098
Immu-Mount mounting medium	Thermo Fisher Scientific (Darmstadt, Germany)	9990402
Coverglass (24 × 60 mm)	Duran Group (Mainz, Germany)	235503704

Material	Manufacturer	Cat. No. (RRID)
Biochemistry		
DAPI	Invitrogen (Darmstadt, Germany)	D1306
ropylene tube with snap-on cap (11 × 39 mm) (1.5 mL)	Beckman Coulter (Krefeld, Germany)	357448
Pierce BCA protein assay kit	Thermo Scientific (Rockford, IL, USA)	23225
NuPAGE LDS sample buffer	Invitrogen (Darmstadt, Germany)	NP0007
10× Bolt sample reducing agent	Invitrogen (Darmstadt, Germany)	B0009
NuPAGE 4–12 % Bis-Tris protein 20-well gels	Invitrogen (Darmstadt, Germany)	NP0321PK2
NuPAGE MOPS running buffer	Invitrogen (Darmstadt, Germany)	NP0001
PageRuler pre-stained protein ladder	Thermo Scientific (Rockford, IL, USA)	26617
Trans-Blot Turbo transfer system	Bio-Rad Laboratories (Feldkirchen, Germany)	1704150
Trans-Blot Turbo mini-2-µm nitrocellulose transfer packs	Bio-Rad Laboratories (Feldkirchen, Germany)	170-4160
V-PLEX pro-inflammatory panel 1 (mouse) kit	Meso Scale Discovery (Rockville, MD, USA)	N05048A-1

Abbreviations: DAPI: 4′,6-diamidino-2-phenylindole, dihydrochloride; BCA: bicinchoninic acid.

2.1.4 Software

Tab. 5: List of software

Software	Manufacturer / original article / URL
Image J	Version 2.0.0.-RC-67/1.52c
Image J Skeletonize (2D/3D) plugin	(Doube et al. 2010) https://imagej.net/Skeletonize3D
Image J Analyze Skeleton (2D/3D) plugin	(Arganda-Carreras et al. 2010) https://imagej.net/AnalyzeSkeleton
IMARIS software	Version 9.5 Oxford Instruments (Oxford, UK)
Surface–surface colocalization XTension	https://imaris.oxinst.com/open/view/surface-surface-colocalization
Image Studio software version 5.2.5	LI-COR Biosciences (Lincoln, NE, USA)
GraphPad Prism software version 9	GraphPad Software (La Jolla, CA, USA)
Adobe Illustrator	Adobe Illustrator 27.4 (Adobe, CA, USA)
Microsoft ware (Office, Excel)	Microsoft 16.72 (Microsoft, NM, USA)
Zotero software	Zotero 6.0.28 (GMU and CHNM, USA)

2.2 Study Approval

The animal care and handling procedures in this study followed the European and German guidelines and were approved by the local government authorities for animal welfare in North Rhine-Westphalia (Folder number 81-02. 04. 2019.A026).

2.2.1 Animals

In this study, we used 6–7-month-old male and female mice on a C57BL/6 mixed genetic background (C57BL/6N and C57BL/6J). Wild type (WT), NLRP3 knockout (KO), and ASC KO mice were used. The control group was treated with sham surgery with the genotype WT mice (mixed C57BL/6N and C57BL/6J) or KO mice, respectively. The KO mice were obtained from Millennium Pharmaceuticals and were previously described (Kanneganti et al., 2006). Specifically, KO mice were created using homologous recombination in embryonic stem cells. In this process, exons I and II of the cryopyrin/Cias1 gene, which

encode the amino-terminal Pyrin domain, were replaced with an IRES-β-gal-neomycin-resistance cassette through a targeting vector. All mice were housed under pathogen-free and standardized conditions with a 12:12-h dark:light cycle at the University Hospital of Bonn and had *ad libitum* access to food and water.

2.2.2 Controlled Skull Impact (CSI) as a Model of Mild Closed Head Injury (CHI)

The CSI model was adapted from the study by Lynch et al. 2005. CSI models an impact similar to a mild CHI. All animals used in this study were operated by Dr. Dr. Sergio Castro-Gomez (**Fig. 2A–C**). The mice were divided into four groups: SHAM-WT, CHI-WT, CHI-NLRP3 KO, and CHI-ASC KO. Anesthesia was induced and maintained using 5 % and continuous inhalation of isoflurane (1.5 %–3 %, 1 L/min), respectively. After deep anesthesia, the mice were fixed in a stereotaxic frame (Stoelting, Dublin, Ireland). To displace the impact force, a 1-mL latex pipette bulb filled with water was placed under the head. A midline sagittal scalp incision was made, and a single controlled midline skull impact was delivered at coordinates of 0.0 mm mediolateral and -1.5 mm anteroposterior, with a velocity of 5 m/s, dwell time of 100 ms, and impact depth of 1.0 mm. This was achieved using a stereotaxic electromagnetic impactor with a 5.0-mm steel tip impounder (Stereotaxic Impactor, Leica Biosystems, Germany). SHAM-injured mice underwent identical surgical procedures as the CHI group, but no impact was delivered. After the operation, mice received the analgesic carprofen (5 mg/kg) subcutaneously once per day and tramadol (1 mg/mL) in drinking water for 3 days post-surgery.

2.2.3 Revised Neurobehavioral Severity Scale (R-NSS)

Dr. Dr. Sergio Castro-Gomez conducted the neurological assessment of the animals using the R-NSS. The R-NSS evaluates the sensory and motor function, reflexes, and balance of the mice. The scale ranges from 0 points to the maximal deficit, with 20 points indicating the most severe symptoms (Yarnell et al., 2016). We used the R-NSS to assess the mice before surgery and at 1, 3, and 7 days after CHI or SHAM surgery (**Fig. 2 D**).

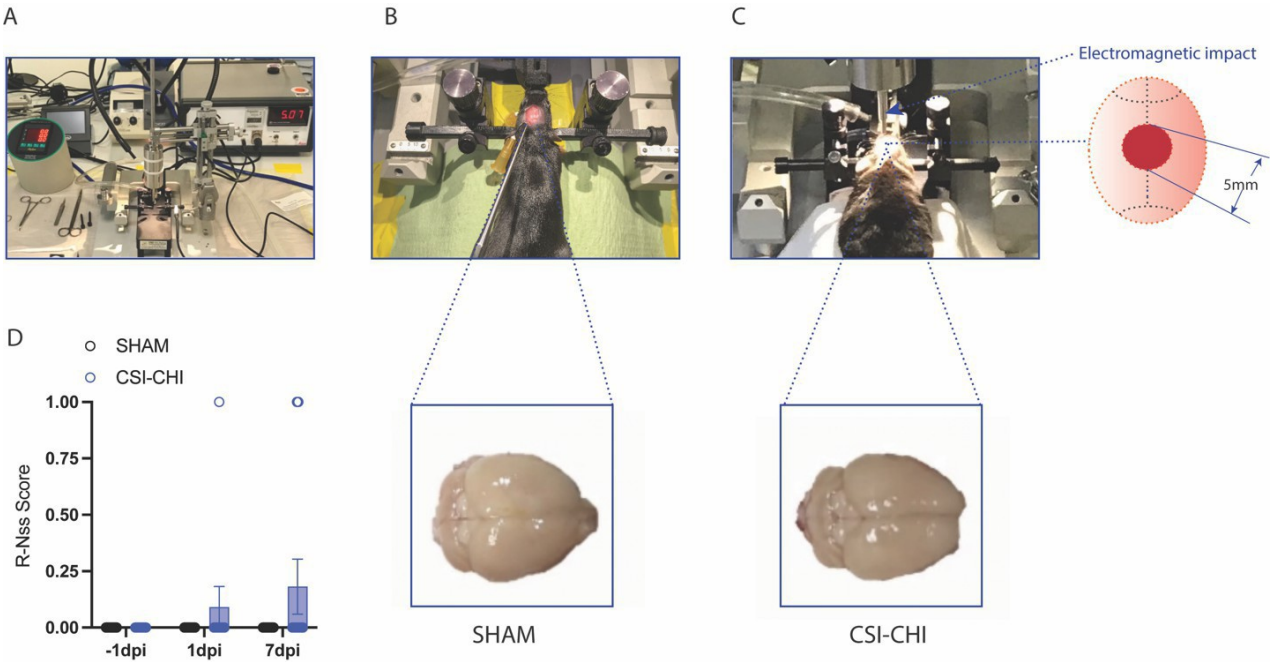

Fig. 2: Controlled Skull Impact as a model for mTBI
A. The CSI-CHI model procedures were performed using a stereotaxic electromagnetic impactor to directly impact the skull. **B.** SHAM-injured mice underwent a midline sagittal scalp incision without impact. **C.** The CHI group mice were delivered a single controlled midline skull impact with a 5.0-mm steel tip after scalp incision. **B–C**. There was no difference in the appearance of the brain tissue between the SHAM and CHI groups, but the CHI group appeared congested. **D.** The R-NSS scores showed no significant difference between the SHAM and CHI groups *(Two-way ANOVA: Time Point, $F(2, 20) = 1.0$, $p = 0.3855$, Trauma effect, $F(1, 10) = 3.7$, $p = 0.0816$. Time Point × Trauma Effect, $F(2, 20) = 1$, $p = 0.3855$; n=11mice, Tukey's multiple comparisons test, $*p < 0.05$. Data are presented as the mean ± SEM.).*

2.3 Histology and Immunohistochemistry

2.3.1 Sample Collection

All perfusions and brain dissections were performed together with Dr. Dr. Sergio Castro-Gomez. Mice from the SHAM and CHI groups at the designated time points (1, 7, and 21 days post-injury [dpi]) were deeply anesthetized with an intraperitoneal injection of a ketamine (100 mg/kg) and xylazine (20 mg/kg) solution and transcranially perfused with ice-cold phosphate-buffered saline (PBS). One of the brain hemispheres was dissected from the skull and fixed overnight with 4 % paraformaldehyde. After 24 hours, the brain samples were washed three times with PBS and then stored in PBS with 0.01 % (w/v) NaN_3 at 4 °C.

2.3.2 Vibratome Sectioning and Immunostaining

Using a Leica VT1000S vibratome, coronal brain sections (40 µm) were cut from the selected brain area between the coordinates -0.45 and -1.85 related to bregma. At least three sections per animal were stained. The sections were washed three times for 5 minutes per wash with PBS and incubated in citrate buffer at 95 °C for 5 minutes. After cooling at room temperature, the sections were washed with PBS and 0.5 % Triton X-100 (PBS-T), followed by blocking with a blocking buffer (10 % [v/v] normal goat serum [Abcam, cat. no. ab7481; RRID: AB_2716553] in PBST) for 1 hour. Next, the sections were incubated overnight at 4 °C with the primary antibodies diluted in blocking solution. The primary antibodies used are listed in **Tab. 2**. The following day, the sections were incubated at room temperature for 1 hour and subsequently incubated with Alexa Fluor 488-, 594-, or 647-conjugated secondary antibodies (1:500) (Invitrogen, Darmstadt, Germany) after three washes with PBS. The sections were then incubated in 0.1 % Sudan Black B (Sigma) in 70 % ethanol for 20 minutes and washed with PBS. Finally, the sections were incubated with DAPI (Invitrogen) for 5 minutes and mounted on slides.

2.3.3 Analysis of ASC Aggregates

The impact area in the cortex was selected for the analysis. Images were captured as Z-Stakes with a step size of 0.5 µm over a depth of 8–10 µm using a confocal LSM900 microscope (Zeiss) with a 40× oil objective (Zeiss). All images used for analysis were taken with the same confocal settings (pinhole: 20, laser intensity: 650, digital gain: 2, and digital offset: -15). The raw .czi files were organized and converted to ims image format using IMARIS (Version 9.5.1). To determine the threshold for detecting ASC specks, at least one positive control (mCherry-ASC mice sample) and one negative control image (ASC-KO mice sample) were used. ASC aggregates were reconstructed using the IMARIS spots tool to set the threshold such that all ASC aggregates would be detected (according to the signal in the positive control), excluding ASC aggregates with less than 1 μm^3 volume (using the negative control to discard possible background). The ASC spot key parameters were carefully defined to ensure accurate detection and analysis. 1) The estimated spot diameter was set at 3 µm for the XY dimension and adjusted to 6 µm for the Z dimension, based on the measured diameter of mCherry-ASC. 2) Background subtraction was applied to reduce noise and enhance the clarity of the spots of interest.

3) A detection quality threshold of 25 was established to ensure that only high-quality spots were identified while minimizing false positives. 4) For spot region selection, local contrast was used with a region border threshold set at 15, allowing precise definition of the ASC signal regions. These parameters were applied to all images. The “Spots Close to Surface” option in IMARIS was used to analyze the distance of ASC aggregates from the microglia surface.

2.3.4 Skeleton Analysis of Microglia and Astrocytes

Image processing was performed using Image J Version 2.0.0.-RC-67/1.52c. Morphological changes in microglia and astrocytes following experimental CHI were analyzed using a computer-assisted cytoskeletal analysis method (Arganda-Carreras et al. 2010). The numbers of process branches, endpoints, and lengths were calculated from the data output of the analyzed skeleton insert, and all data (branches/cell, endpoints/cell, and process lengths/cell) in each image were normalized by the number of cells per image.

2.3.5 Contact Analysis Between Microglia and Astrocytes

IMARIS was used to create 3D surfaces representing the microglia and astrocytes by setting a threshold for the signal intensity. To set the parameters for the surface of microglia and astrocytes in Imaris, first load the dataset and access the 'Surfaces' tool. Adjust the smoothing factor (typically 0.368 µm) to balance surface detail and noise reduction and set the intensity threshold manually (range from 12.5 to 14.5) for optimal surface detection. The surface–surface colocalization extension was used to determine the cellular area in contact between the microglial surface and the astrocytic surface. This extension masks each of the two cellular surfaces and identifies the overlapping voxels within each surface, generating a new surface from the overlapping regions where the contact area (μm^2) is calculated.

2.3.6 IL-1β Analysis of the Cortex

To identify the possible source of IL-1β in the lesioned cortex, co-immunostaining for IL-1β, Iba1, GFAP, and NeuN within the peri-contusional cortex was conducted in two separate experiments at 7 and 21 dpi. The same spot threshold parameter used for ASC analysis was applied to all images. The surfaces of microglia, astrocytes, and neurons were reconstructed, and the “Spots Close to Surface” tool in IMARIS was used to analyze

the distance of IL-1β signals from these surfaces. The numbers of IL-1β spots in microglia, astrocytes, and neurons were quantified.

2.4 Tissue Protein Extraction and Immunoblotting

After transcardial perfusion with cold PBS, the right hemisphere was dissected, snap frozen in liquid nitrogen, and stored at -80 °C. The tissue was homogenized in homogenization buffer (PBS, 5 mM NaF, 20 mM pyrophosphate, and 1 mM AEBSF and 1:100 protease inhibitor cocktail) using a tissue homogenizer (Precellys 24) for 30 seconds. The homogenized tissue was then mixed with 2× RIPA buffer (25 mM Tris-HCl [pH 7.5], 150 mM NaCl, 1 % Nonidet P-40, 0.5 % NaDOC, 0.1 % SDS). After sonication (10 seconds, 80 % duty, 12 % power) and ultracentrifugation (100,000 × *g* for 30 minutes at 4 °C), the supernatant was collected. The protein concentration in the supernatant was determined using a BCA assay (Thermo Fisher Scientific). The samples were mixed with 1× NuPAGE sample buffer (Thermo Fisher Scientific) and heated for 5 minutes at 95 °C. Subsequently, the samples were separated on 4 %–12 % NuPAGE Novex gels (Thermo Fisher Scientific) and transferred to nitrocellulose membranes for immunoblotting. The antibodies used are listed in **Tab. 1**. The immunoreactivity was detected using an Odyssey CLx imager (Licor, Bad Homburg, Germany), and the images were analyzed using ImageStudio software version 5.2.5 (LI-COR).

2.5 ELISA Pro-inflammatory Cytokine Panel

well and incubated at room temperature for 2 hours under constant shaking. After another wash step, 150 µ of read buffer were added to each well. The optical density of the content of each well was determined using a MESO QuickPlex SQ 120MM (Meso Scale Discovery, Rockville, MD, USA).

The levels of cytokines (IL-1β, IL-2, IL-4, IL-5, IL-6, IL-10, IL-12 p20, TNF-α, KC/GRO, and INF-γ) in brain lysates were determined using the V-PLEX Plus Pro-inflammatory Panel 1 (mouse) Kit, following the manufacturer's instructions (Meso Scale Discovery, Rockville, MD, USA). Briefly, 25 µl of samples or standards diluted in reagent diluent 41 (1:1) were added to each well of the plate. The plate was covered with an adhesive strip and incubated at room temperature for 3 hours under constant shaking. The well contents were aspirated and washed three times with 150 µl of wash buffer for 5 minutes per wash.

Then, 25 µ of detection antibodies diluted in reagent diluent 45 (1:50) were added to each.

2.6 Statistical Analysis

All statistical analyses were conducted using GraphPad Prism 9 (GraphPad Software, CA, USA). Data normality was assessed using the Shapiro–Wilk test. When data met the assumption of a Gaussian distribution, parametric tests were applied; otherwise, non-parametric alternatives were used.

To evaluate the effects of genotype and time, a two-way repeated measures analysis of variance (ANOVA) was performed, followed by Bonferroni's multiple comparisons test to correct for multiple comparisons. This approach was selected due to its suitability for analyzing interactions between two independent variables in repeated-measures designs. Two-tailed t-tests were also used for overall comparisons of target parameters between genotypes.

For most parameter comparisons—including Western blot quantifications, glial cell populations, cell counts, ASC fluorescence intensity, IL-1β expression, morphological assessments, and microglial contact area —we used a two-way ANOVA with Bonferroni's multiple comparisons test and a two-tailed t-test. Data are presented as mean ± standard error of the mean (SEM) in the figures. Statistical significance is indicated as $*p < 0.05$, $**p < 0.01$, $***p < 0.001$, and $****p < 0.0001$.

Additionally, Pearson correlation analysis was used to explore the relationship between ASC fluorescence intensity and the microglial contact area.

3. Results

3.1 NLRP3 Inflammasome-related Proteins Are Upregulated Following Head Injury

To examine the expression of NLRP3-related inflammasome proteins, we performed western blot analysis of the cortices from WT, NLRP3 KO, and ASC KO mice that underwent either SHAM or CHI surgery at 1, 7, and 21 dpi. We specifically analyzed the protein levels of NLRP3, ASC, CASP-1, and IL-1β (**Fig. 3A–B**). Our results showed that the expression levels of ASC, NLRP3, and pro-CASP-1 *(Bonferroni's multiple comparisons test, dpi $F(3,24)$, $^{*}p < 0.05$)* significantly increased over time (**Fig. 3E, F, G, I**), indicating a whole upregulation of NLRP3 inflammasome components. Additionally, the expression of the cleaved form of CASP-1 peaked at 21 dpi. Notably, the levels of cleaved CASP-1 and IL- 1β were higher at 21 dpi than at 7 dpi (**Fig. 3C, D, G, H**), suggesting that the inflammasome may exhibit a higher level of activation and pro-inflammatory activity at 21 dpi than at 7 dpi.

Next, we evaluated the effect of NLRP3 and ASC genetic deficiency in mTBI. Our findings showed that both NLRP3 KO and ASC KO reduced the expression of NLRP3- related proteins (**Fig. 3C–J**). Notably, ASC KO mice *(WT 21 dpi vs. ASC KO 21 dpi, Bonferroni's Test $^{**}p = 0.0016$; t-Test $^{**}p = 0.0079$)* showed a more obvious downward trend in the expression of cleaved CASP-1 than NLRP3 KO mice *(WT 21 dpi vs. NLRP3 KO 21 dpi, Bonferroni's Test $^{**}p = 0.0099$; t-Test $p = 0.0579$)*. While both ASC KO *(WT 21 dpi vs. ASC KO 21 dpi, Bonferroni's Test $^{**}p = 0.0015$)* and NLRP3 KO *(WT 21 dpi vs. NLRP3 KO 21 dpi, Bonferroni's Test $^{*}p = 0.0236$)* mice showed noticeably downregulated expression of cleaved IL-1β at 21 dpi compared with the WT group. Furthermore, ASC KO mice demonstrated a more influence on the regulation of IL-1β, compared with NLRP3 KO group. (**Fig. 3C, D, G, H**).

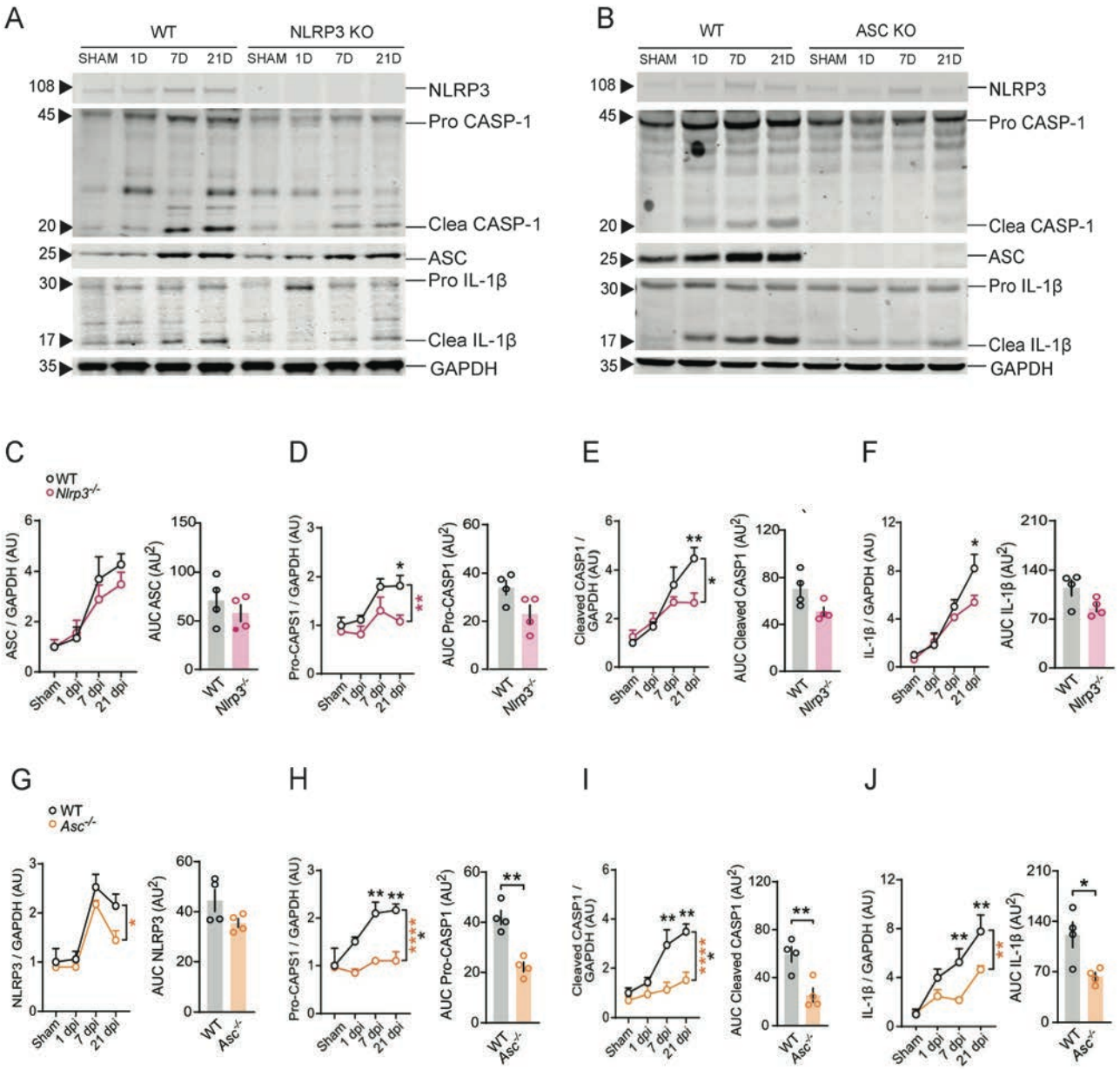

Fig. 3: NLRP3 inflammasome-related proteins are persistently increased following mTBI **A–B.** Representative western blot images and densitometric semi-quantification of NLRP3, ASC, CASP-1, and IL-1β at 1, 7, and 21 dpi in the peri-contusional cortices of mice subjected to SHAM surgery or CHI. **C–F.** The expression of target proteins (NLRP3, ASC, Pro-CASP-1, cleaved CASP-1, and cleaved IL-1β) was analyzed in WT and NLRP3 KO group. **G-J.** The expression of target proteins was analyzed in WT and ASC KO group. **C-J.** ***Left panel:*** *Two-way ANOVA, Bonferroni's multiple comparisons test. AU, arbitrary units;* ***Right panel:*** *Two-tailed t-tests represent integrated relative concentrations. AUC, Area Under Curve. n = 4 mice /group, *p < 0.05, **p < 0.01, ***p < 0.001, ****p < 0.0001. Data are presented as the mean ± SEM. dpi, days post-injury.*

3.2 Iba1$^+$ Cells Were the Primary Cellular Source of IL-1β Following mild Traumatic Brain Injury

To examine the potential release of pro-inflammatory markers associated with the expression of NLRP3 inflammasome-related proteins after injury, we conducted an ELISA–Multiplex assay (V-PLEX pro-inflammatory panel 1 (mouse) kit, Rockville, MD, USA) on the lysates of lesioned cortices from WT, NLRP3 KO, and ASC KO mice at 1, 7, and 21 dpi. Our findings revealed a significant increase in IL-1β expression at 21 dpi, and this increase was inhibited by NLRP3 and ASC KO *(Bonferroni's multiple comparisons test, dpi F(3,18) , ****p <0.0001, WT 21 dpi vs. KO 21 dpi, ****p <0.0001)* (**Fig. 4A**). Notably, mice with ASC KO *(*t-Test, ****p = 0.0001)* exhibited a more pronounced reduction in the expression of IL-1β compared to those with NLRP3 KO(t-Test, ***p = 0.0039*) (**Fig. 4E**). Similarly, TNF-α levels were significantly upregulated at 21 dpi, which could be reversed by ASC and NLRP3 KO with statistical significance *(Bonferroni's multiple comparisons test, dpi F(3,18) , ****p <0.0001, WT 21 dpi vs. KO 21 dpi, ***p =0.0001)* (**Fig. 4F**). Meanwhile, we observed an increasing trend in the expression of IL-6 over time, and ASC plays a role in regulating IL-6 expression *(Two-way ANOVA: Genotype, F (1, 18) = 11.48, **p = 0.0033)* (**Fig. 4C, G**). The other cytokines in the panel did not exhibit any statistically significant changes.

Next, we investigated the cellular sources of IL-1β expression using immunohistochemical staining for IL-1β, Iba1, GFAP, and NeuN in the peri-contusional cortices of mice at 7 and 21 dpi (**Fig. 4H-I**). At 7 days post-mTBI, approximately 16 % of the IL-1β signal was found to be colocalized with or in the vicinity of GFAP (presumably astrocytes), 74 % in Iba1-positive cells (likely microglia), and 9 % near NeuN (likely Neuron) *(Iba1$^+$ cell: 16.16 % ± 2.542 %; GFAP$^+$ cell: 74.91% ± 2.542 %; NeuN$^+$ cell: 9.02 % ± 2.87 %)* (**Fig. 4J**).

Interestingly, at 21 dpi, the majority of IL-1β (approximately 60 %) was found in Iba1-positive cells (microglia or infiltrating macrophages), while around 30 % was found in GFAP-positive cells and 10 % in the vicinity of NeuN-positve cells *(Iba1$^+$ cells: 60.22% ± 2.542 %; GFAP$^+$ cells: 29.73 % ± 2.542 %; NeuN$^+$ cells: 10.43 % ± 2.87 %)* (**Fig. 4J**). Notably, the number of IL-1β spots within both Iba1-positive and GFAP-positive cells was significantly increased at 21 dpi compared with 7 dpi *(Two-way ANOVA, Bonferroni's multiple comparisons test, Iba1$^+$ cells 21 dpi vs. 7 dpi, ****p < 0.0001; GFAP$^+$ cells 21 dpi*

*vs. 7 dpi, *p = 0.0372)* (**Fig. 4K**).

Our findings thus emphasize the roles of NLRP3 and ASC, particularly the crucial role of ASC, in triggering inflammatory factors. Moreover, Iba1-positive cells, likely microglia, or infiltrating macrophages, were found to be the primary cellular sources of IL-1β at 21 dpi.

Fig. 4: IL-1β and TNF-α were upregulated at 21 days after closed head injury, with Iba 1^+ cells being the predominant cell subset responsible for the expression of IL-1β
A, B, F, G. ELISA–Multiplex assay revealed an upregulation of IL-1β and TNF-α expression at 7 dpi, with a significant increase at 21 dpi. This increase was significantly reduced in KO mice. **C, E.** IL-6 expression gradually increased following the injury, and ASC KO downregulated this increased IL-6 expression. **A-G**. ***Left panel:*** *Two-way ANOVA, Bonferroni's multiple comparisons test;* ***Right panel:*** *Two-tailed t-tests represent integrated relative concentrations. AUC, Area Under Curve. n = 12 slice (4 mice)/group, *p < 0.05, **p < 0.01, ***p < 0.001, ****p < 0.0001. Data are presented as the mean ± SEM.* **H–I**. Representative images of immunohistochemical staining of the peri-contusional cortices for IL-1β**,** Iba1, GFAP, and NeuN at 7 and 21 dpi. IMARIS was used for the IL-1β analysis. Scale bar = 20 μm. **J.** The percentage of IL-1β expression was assessed in Iba1-positive cells, GFAP-positive cells, and NeuN-positive cells at both 7 dpi and 21 dpi *(n = 12 slice (4 mice) /group. Data are presented as the mean ± SEM.)*. **K.** The levels of IL-β expression in Iba1-positive cells and GFAP-positive cells was significantly increased at 21 dpi compared with 7 dpi *(Two-way ANOVA, Bonferroni's multiple comparisons test, *p < 0.05, **p < 0.01, ***p < 0.001, ****p < 0.0001, n = 12 slice (4 mice) /group. Data are presented as the mean ± SEM.)*.

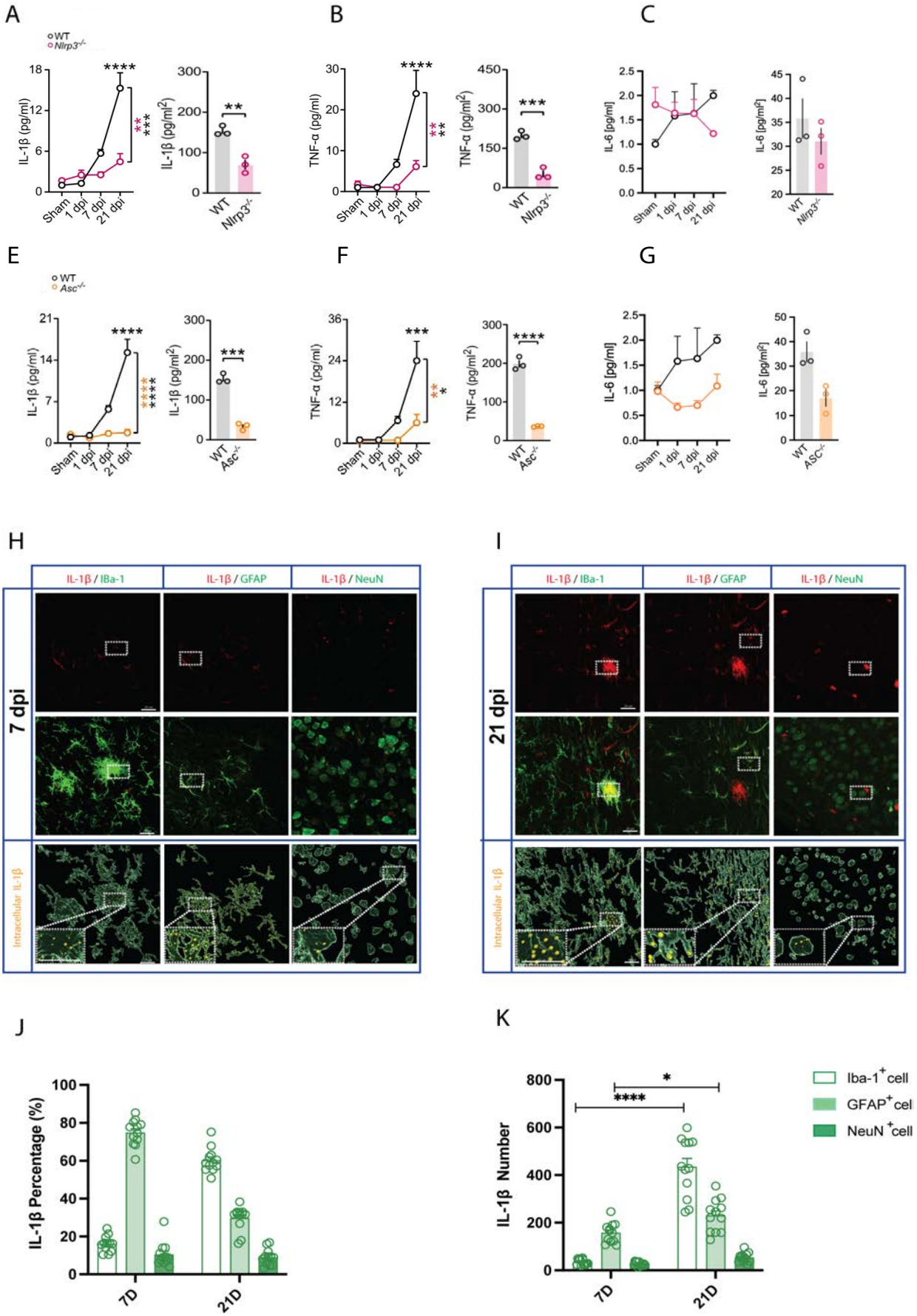
A
B
C
WT
Nlrp3-/-
IL-1β (pg/ml)
IL-1β (pg/ml²)
TNF-α (pg/ml)
TNF-α (pg/ml²)
IL-6 [pg/ml]
IL-6 [pg/ml²]
Sham
1 dpi
7 dpi
21 dpi
E
F
G
Asc-/-
H
I
IL-1β / IBa-1
IL-1β / GFAP
IL-1β / NeuN
7 dpi
21 dpi
Intracellular IL-1β
J
K
IL-1β Percentage (%)
IL-1β Number
7D
21D
Iba-1+cell
GFAP+cel
NeuN +cell

3.3 NLRP3 Regulates ASC Aggregation Within Iba1+ cells Following mild Traumatic Brain Injury

We confirmed the significant expression of CASP-1 and cytokines (IL-1β and TNF-α) at 21 dpi. To explore the potential involvement of post-traumatic inflammasomes within the microglia or infiltrating macrophages, we conducted immunohistochemical staining of the contusional cortical tissue for the inflammasome adaptor protein ASC and Iba1 at 1, 7, and 21 dpi in comparison with SHAM mice as proxy for inflammasome activation. The microglial surface reconstruction and ASC immunosignal spot analysis was conducted using IMARIS (**Fig. 5A–B**).

3.3.1 Distinct Patterns of ASC Expression in the WT and NLRP3 KO Groups

We detected that the total number of fluorescent ASC spots increased significantly in microglia at 7 dpi and peaked at 21 dpi (*Bonferroni's multiple comparisons test, dpi F(2,66) , ****p <0.0001*) (Fig. 5C). Meanwhile, the number of ASC spots within Iba1+ cells followed a similar pattern to the total number of ASC spots (*Bonferroni's test, dpi F(2,66) , ****p <0.0001*) (**Fig. 5D**). It is noteworthy that in the NLRP3 KO group, no significant reduction was observed in the total number of ASC spots or the intracellular ASC count (**Fig. 5C–D**). Interestingly, the number of ASC spots outside of Iba1^{+} cells increased at 7 dpi and showed a significant increase at 21 dpi in both WT and NLRP3 KO mice. However, the number of extracellular ASC spots In the NLRP3 KO group was significantly decreased compared with the WT group *(WT 21 dpi vs. NLPR3 KO 21 dpi, ****p < 0.0001)* (**Fig. 5E**).
ASC Aggregation Within Iba1+ Cells Differs Between the WT and NLRP3 KO Group.
Furthermore, we observed that as the number of ASC spots increased within microglia, there was a corresponding increase in their volume, as depicted in the magnified IMARIS images (**Fig. 5A–B**). To quantitatively analyze ASC aggregation, we divided the volume of ASCs into three categories (1–20 um³, 20–30 um³, 30–40 um³) and counted the number of ASC spots in each category for statistics (**Fig. 5F–H**). We observed that the number of ASC spots in the 1–20 um³ range increased at 1 dpi and surged remarkably at 7 dpi and 21 dpi in both the WT and NLRP3 KO groups (**Fig. 5F**). Meanwhile, the number of ASC spots in the 20–30 um³ range increased significantly at 7 dpi and 21 dpi in the WT group and showed a similar significant increase at 21 dpi in the NLRP3 KO group (**Fig. 5G**). Intriguingly, ASC spots in

the 30–40 um³ range were predominantly found at 21 dpi in the WT group, while their number was significantly decreased in the NLRP3 KO group at the same time point *(Bonferroni's multiple comparisons test, WT 21 dpi vs. NLRP3 KO 21 dpi, ***p = 0.0006. t-Test, WT vs. NLRP3 KO, **p = 0.008)* (**Fig. 5H**).

Collectively, our findings illustrate a remarkable upregulation of extracellular ASC, coupled with a substantial aggregation of ASC within microglia or infiltrating macrophages at 21 dpi, in the WT group. In contrast, the NLRP3 KO group displayed a milder aggregation of ASC within Iba1$^+$ cells and fewer extracellular ASC spots than the WT group at 21 dpi. These observations highlight the potentially essential role of NLRP3 in promoting the expression of extracellular ASC and facilitating significant ASC aggregation at 21 dpi following brain injury.

Fig. 5: NLRP3 contributes to extracellular ASC upregulation and ASC aggregation within Iba1$^+$ cells at 21 dpi following mTBI

A–B. Representative images of immunohistochemical staining of the peri-contusional cortices for Iba1 (green) and ASC (red) at 1, 7, and 21 dpi, with ASC analysis conducted using IMARIS (Scale bar = 20 μm). **C–E.** The number of ASC fluorescent spots was analyzed in both the WT and NLRP3 KO groups *(**Left panel:** Two-way ANOVA, Bonferroni's multiple comparisons test; **Right panel:** Two-tailed t-tests represent integrated relative concentrations. AUC, Area Under Curve. n = 12 slice (4 mice)/group, *p < 0.05, **p < 0.01, ***p < 0.001, ****p < 0.0001. Data are presented as the mean ± SEM* **)**. **F–H**. The volume of ASC aggregation is divided into three grades (1–20 um^3, 20–30 um^3, 30– 40 um^3) for statistics *(**Left panel:** Two-way ANOVA, Bonferroni's multiple comparisons test; **Right panel:** Two-tailed t-tests represent integrated relative concentrations. AUC, Area Under Curve. n = 12 slice (4 mice)/group, *p < 0.05, **p < 0.01, ***p < 0.001, ****p < 0.0001. Data are presented as the mean ± SEM* **).**

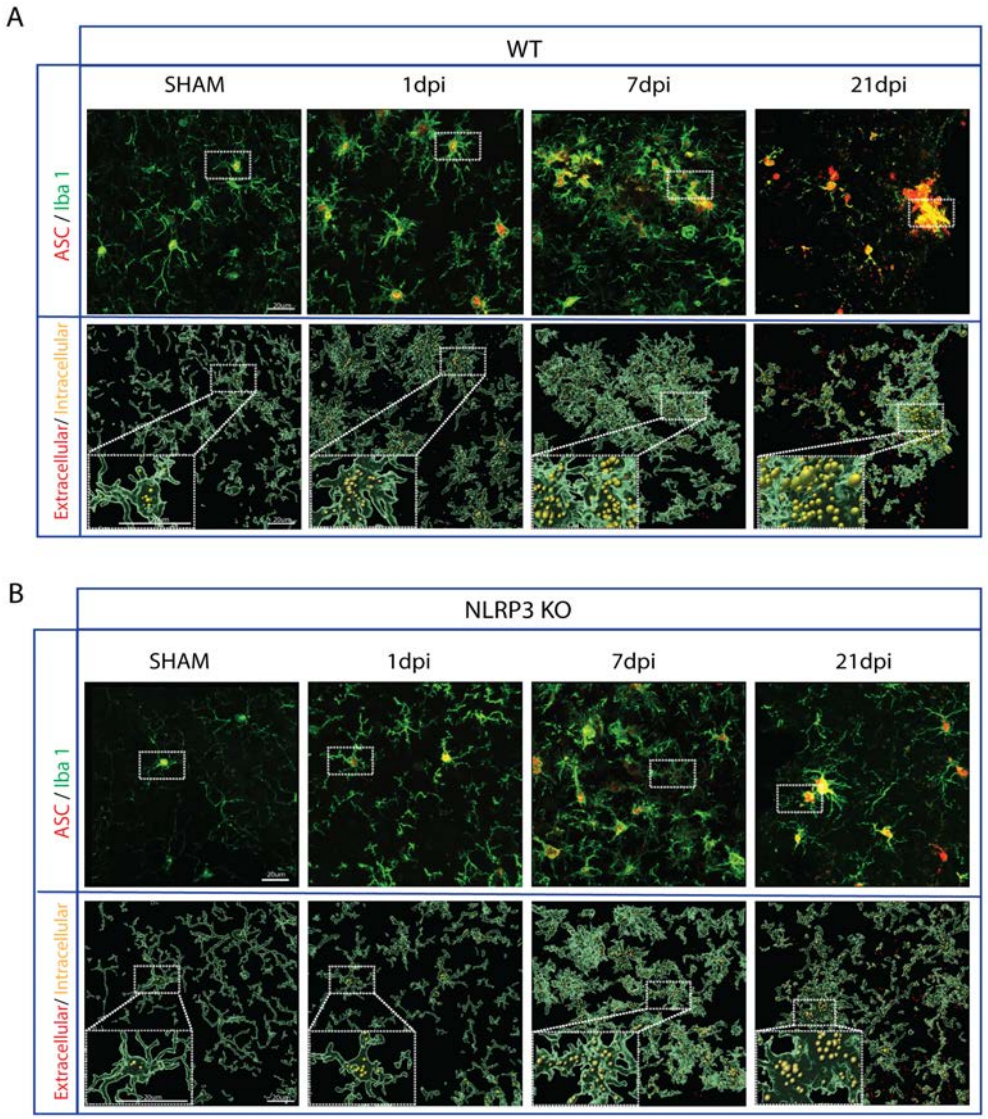
A
WT
SHAM
1dpi
7dpi
21dpi
ASC / Iba 1
Extracellular/ Intracellular
B
NLRP3 KO
SHAM
1dpi
7dpi
21dpi
ASC / Iba 1
Extracellular/ Intracellular

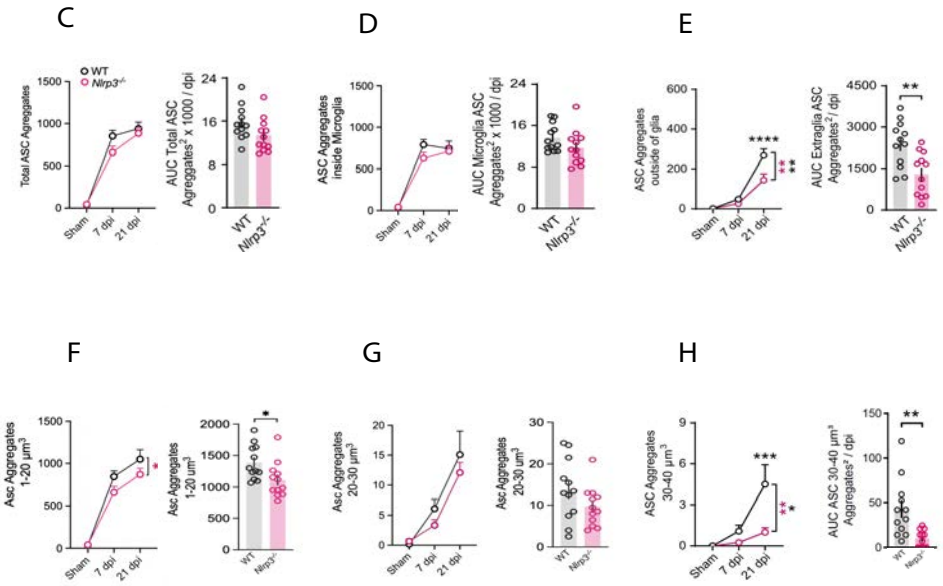
C
D
E
WT
Nlrp3-/-
Total ASC Agregates
AUC Total ASC Agregates² x 1000 / dpi
ASC Aggregates inside Microglia
AUC Microglia ASC Agregates² x 1000 / dpi
ASC Aggregates outside of glia
AUC Extraglia ASC Aggregates² / dpi
Sham
7 dpi
21 dpi
F
G
H
Asc Aggregates 1-20 µm³
Asc Aggregates 20-30 µm³
ASC Aggregates 30-40 µm³
AUC ASC 30-40 µm³ Aggregates² / dpi

3.4 NLRP3 and ASC Contribute to the Morphological Alterations Observed in Iba1+ Cells after mild Traumatic Brain Injury

Microglia exhibit distinct adaptive morphologies in response to traumatic stimuli (Savage et al. 2019, Szabo and Gulya 2013). To investigate the morphological changes in Iba1$^+$ cells, we performed immunofluorescence staining for Iba1 and employed skeleton analysis to examine the contusional cortices of WT, NLRP3 KO, and ASC KO mice at 1, 7, and 21 dpi (**Fig. 6A–B**).

First, we observed a significant increase in the Iba1$^+$ cell count at 7 dpi in both WT and NLRP3 KO mice *(Bonferroni's multiple comparisons test, dpi F(3,88) ****p < 0.0001)* (**Fig. 6C**). However, in ASC KO mice, the cell count decreased significantly compared with WT mice at 7 dpi (*Bonferroni's multiple comparisons test, WT 7dpi vs. ASC KO7 dpi, *p = 0.015*) (Fig. 6G). Subsequently, we quantified the normalized changes in the morphology of Iba1+ cells based on the cell count. The morphological alterations, including the number of branches per cell, endpoints per cell, and branch length per cell significantly decreased after injury, particularly at 21 dpi *(Bonferroni's multiple comparisons test, dpi F(3,88) ****p < 0.0001)*. Meanwhile, NLRP3 KO exhibited a relieving effect on these changes *(Bonferroni's multiple comparisons test, WT 21dpi vs. NLRP3 KO21 dpi *p < 0.05, **p < 0.01)* (**Fig. 6D–F**). Notably, ASC KO mice showed a significant alleviation of the morphological alterations at 21 dpi compared with WT mice *(Bonferroni's multiple comparisons test, WT 21dpi vs. ASC KO21 dpi **p < 0.01, ***p < 0.001,)* (**Fig. 6H–J**). In conclusion, our observations revealed a progressive debranching of Iba1$^+$ cells over time following injury, with the cells significantly shrinking by 21 dpi. Notably, the KO groups, especially the ASC KO group, exhibited a reversal of these cellular morphological alterations. In addition to the morphological changes, we noted significant changes in the spatial distribution of Iba1$^+$ cells. In the WT group, Iba1$^+$ cells appeared to gradually move closer to each other, eventually clustering and merging to form multinucleated giant cells at 21 dpi (**Fig. 6K**).

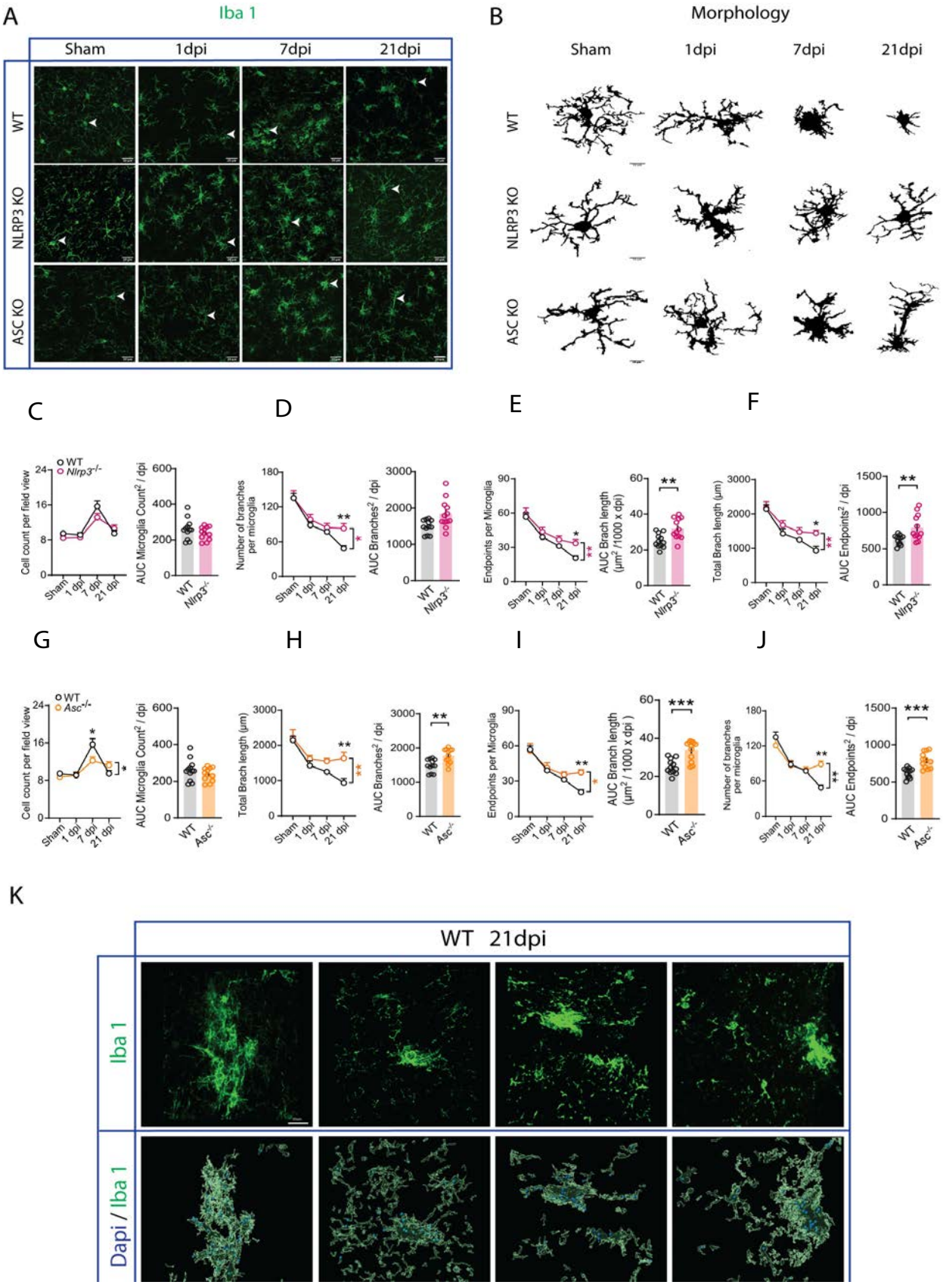
A
Iba 1
Sham
1dpi
7dpi
21dpi
WT
NLRP3 KO
ASC KO
B
Morphology
C
D
E
F
G
H
I
J
K
WT 21dpi
Iba 1
Dapi / Iba 1

Fig. 6: Morphological changes in Iba1$^+$ cells following mTBI
A. Representative images of immunohistochemical staining for Iba1 (green) in WT, NLRP3 KO, and ASC KO mice at 1, 7, and 21 dpi. The arrows indicate representative morphologies at various post-injury time points. Scale bar = 20 μm. **B.** The representative Iba1$^+$ cell morphologies processed with skeleton analysis. Scale bars = 10 μm. The morphology of microglia exhibited a gradual debranching over time following injury, and by 21 dpi, the cells had even shrunk. **C-F.** The cell count, branches per cell, endpoints per cell, and process lengths per cell were analyzed in the WT and NLRP3 KO groups *(**Left panel:** Two-way ANOVA, Bonferroni's multiple comparisons test; **Right panel:** Two-tailed t-tests represent integrated relative concentrations. AUC, Area Under Curve. n = 12 slice (4 mice)/group, *p < 0.05, **p < 0.01, ***p < 0.001, ****p < 0.0001. Data are presented as the mean ± SEM* **). G-J.** The cell count, branches per cell, endpoints per cell, and process lengths per cell were analyzed in the WT and ASC KO groups *(**Left panel:** Two-way ANOVA, Bonferroni's multiple comparisons test; **Right panel:** Two-tailed t-tests represent integrated relative concentrations. AUC, Area Under Curve. n = 12 slice (4 mice)/group, *p < 0.05, **p < 0.01, ***p < 0.001, ****p < 0.0001. Data are presented as the mean ± SEM* **). K.** Using IMARIS, we observed the fusion of Iba1$^+$ cells with the aggregation of multiple cell nuclei at 21 dpi in the WT group. Scale bar = 20 μm.

3.5 The Morphology of GFAP$^+$ Cells Synchronized with that of Iba1$^+$ Cells after Brain Injury

Studies have provided evidence that morphological changes in astrocytes are intricately linked to microglia during inflammation-induced responses (Liddelow and Barres 2017; Althammer et al. 2020). GFAP serves as a classical biomarker for assessing astrocyte morphology in the CNS, commonly employed in the context of TBI (Wang et al. 2018b). To examine the morphological alterations in GFAP$^+$ cells following mTBI, we conducted a morphological analysis similar to that performed for Iba1$^+$ cells (**Fig. 7A–B**). We initially observed a noteworthy increase in the count of GFAP$^+$ cells at 1 and 7 dpi in WT mice(*Bonferroni's multiple comparisons test, dpi F(3,88) ****p < 0.0001*), and this increase was suppressed by ASC KO at 7 dpi *(Bonferroni's multiple comparisons test, *p = 0.025)* (**Fig. 7C**). And ASC KO also exerted a genotype-related effect in inhibiting the increase in cell count *(Two-way ANOVA: Genotype, F (1, 81) = 8.467, **p = 0.0046)*. (**Fig. 7G**). Subsequently, we quantified normalized changes in the morphology of GFAP$^+$ cells based on the cell count. The branches per cell, endpoints per cell, and length of branches per cell were significantly decreased after head injury, particularly at 21 dpi(*Bonferroni's multiple comparisons test, dpi F(3,88) ****p < 0.0001*). NLRP3 KO alleviated these morphological alterations (*Bonferroni's multiple comparisons test, WT 21dpi vs. NLRP3*

*KO21 dpi *p < 0.05, **p < 0.01)* (**Fig. 7D–F**). However, ASC KO significantly alleviated these morphological changes at 21 dpi compared with WT mice *(Bonferroni's multiple comparisons test, WT 21dpi vs. NLRP3 KO21 dpi **p < 0.01, ***p < 0.001,)* (**Fig. 7H–J**). Notably, in terms of spatial distribution, we observed that multiple GFAP$^+$ cells aggregated and fused together at 21 dpi (**Fig. 7K**). Similar morphological changes to those in microglia were also observed in astrocytes after injury, suggesting a potential correlation between these two types of glial cells.

Fig. 7: Morphological changes in GFAP$^+$ cells
A. Representative images depict immunohistochemical staining for GFAP (magenta). Scale bar = 20 μm. The white arrows are used to indicate representative morphologies observed at various post-injury time points. The yellow arrow shows a giant GFAP$^+$ tissue. **B.** The skeleton analysis for representative GFAP $^+$ cell morphologies. Scale bar = 10 μm. **C-F.** The cell count, branches per cell, endpoints per cell, and process lengths per cell were analyzed in the WT and NLRP3 KO groups *(**Left panel:** Two-way ANOVA, Bonferroni's multiple comparisons test; **Right panel:** Two-tailed t-tests represent integrated relative concentrations. AUC, Area Under Curve. n = 12 slice (4 mice)/group, *p < 0.05, **p < 0.01, ***p < 0.001, ****p < 0.0001. Data are presented as the mean ± SEM* **). G-J.** The cell count, branches per cell, endpoints per cell, and process lengths per cell were analyzed in the WT and ASC KO groups *(**Left panel:** Two-way ANOVA, Bonferroni's multiple comparisons test; **Right panel:** Two-tailed t-tests represent integrated relative concentrations. AUC, Area Under Curve. n = 12 slice (4 mice)/group, *p < 0.05, **p < 0.01, ***p < 0.001, ****p < 0.0001. Data are presented as the mean ± SEM* **). K.** IMARIS was used to observe GFAP$^+$ cells fused with aggregated multiple cell nuclei at 21 dpi in the WT group. Scale bar = 20 μm.

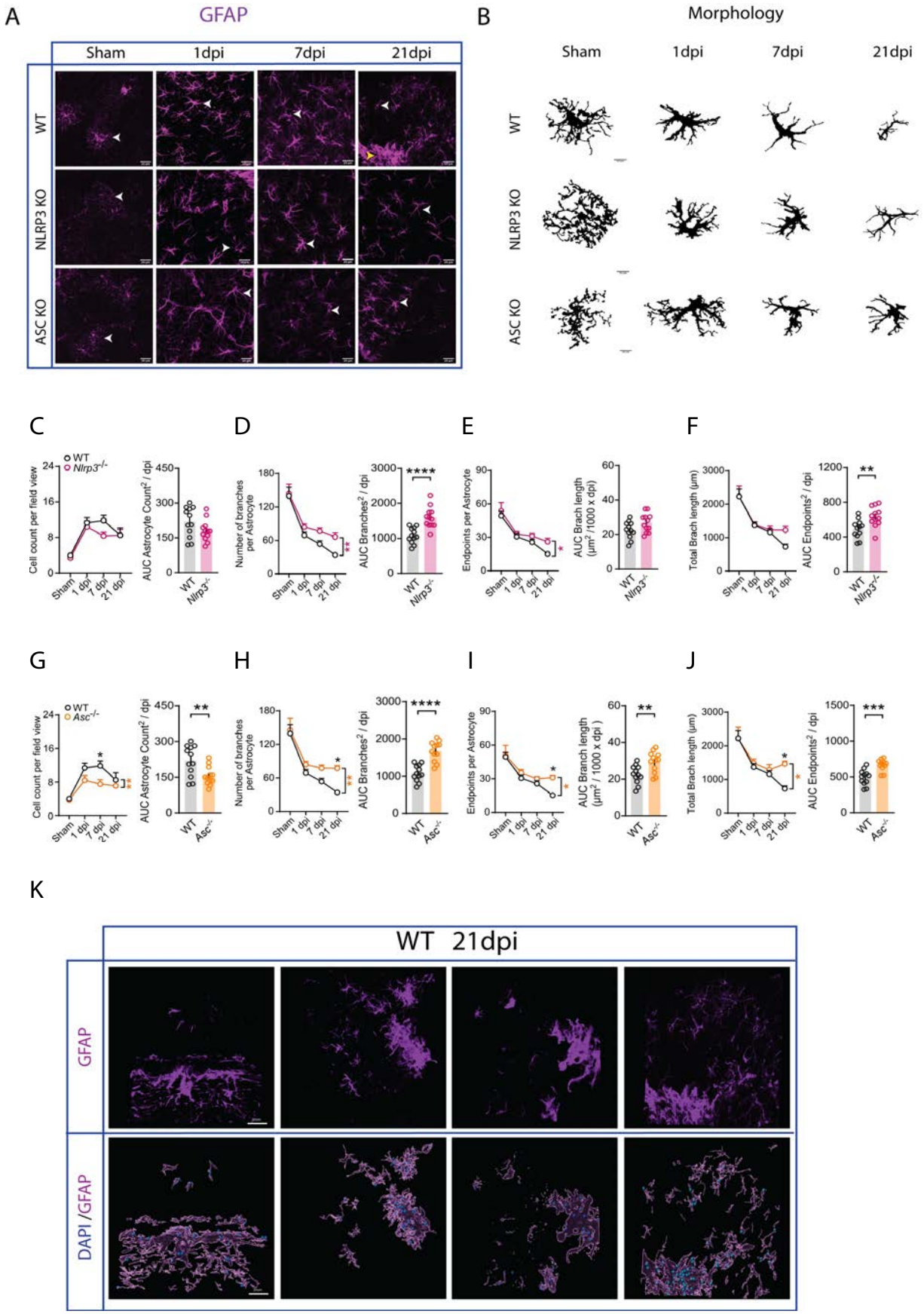
A
GFAP
Sham
1dpi
7dpi
21dpi
WT
NLRP3 KO
ASC KO
B
Morphology
Sham
1dpi
7dpi
21dpi
WT
NLRP3 KO
ASC KO
C
D
E
F
WT
Nlrp3-/-
Cell count per field view
AUC Astrocyte Count² / dpi
Number of branches per Astrocyte
AUC Branches² / dpi
Endpoints per Astrocyte
AUC Brach length (µm² /1000 x dpi)
Total Brach length (µm)
AUC Endpoints² / dpi
Sham
1 dpi
7 dpi
21 dpi
G
H
I
J
WT
Asc-/-
Cell count per field view
AUC Astrocyte Count² / dpi
Number of branches per Astrocyte
AUC Branches² / dpi
Endpoints per Astrocyte
AUC Branch length (µm² / 1000 x dpi)
Total Brach length (µm)
AUC Endpoints² / dpi
K
WT 21dpi
GFAP
DAPI /GFAP

3.6 ASC Upregulation Contributes to the Morphological Contact of Glial Cells

3.6.1 Contact Between Glial Cells in the Absence of NRLP3 and ASC

To investigate the potential interaction between astrocytes and microglia following injury, we performed surface–surface colocalization analysis of the contact area (μm^2) with IMARIS **(Fig. 8A–C)**. We observed a significant increase in the contact area between microglia and astrocytes at 7 dpi, reaching a peak at 21 dpi in WT mice *(Bonferroni's multiple comparisons test, dpi F(2,66) ****p < 0.0001)*. Notably, the contact volume decreased significantly at 21 dpi in NLRP KO mice *(WT 21 dpi vs. NLRP3 21 dpi, **p = 0.0017)* and particularly in ASC KO mice *(WT 21 dpi vs. ASC KO 21 dpi, ****p < 0.0001)* **(Fig. 8D–E)**.

Fig. 8: NLRP3 and ASC play different roles in enhancing the contact between $Iba1^+$ cells and $GFAP^+$ cells
A–C. Representative image of immunohistochemical staining for Iba1 (green) and GFAP (magenta) in the peri-contusional cortex. The surface–surface colocalization X Tension program in IMARIS was used to analyze the contact area between Iba1+ cells and GFAP+ cells in the WT, NLRP3 KO, and ASC KO groups. Scale bar = 20 µm. D–E. The contact area showed a significant increase at 21 dpi, while it decreased significantly after NLRP3 KO and especially after ASC KO *(**Left panel:** Two-way ANOVA, Bonferroni's multiple comparisons test; **Right panel:** Two-tailed t-tests represent integrated relative concentrations. AUC, Area Under Curve. n = 12 slice (4 mice)/group, *p < 0.05, **p < 0.01, ***p < 0.001, ****p < 0.0001. Data are presented as the mean ± SEM* **).**

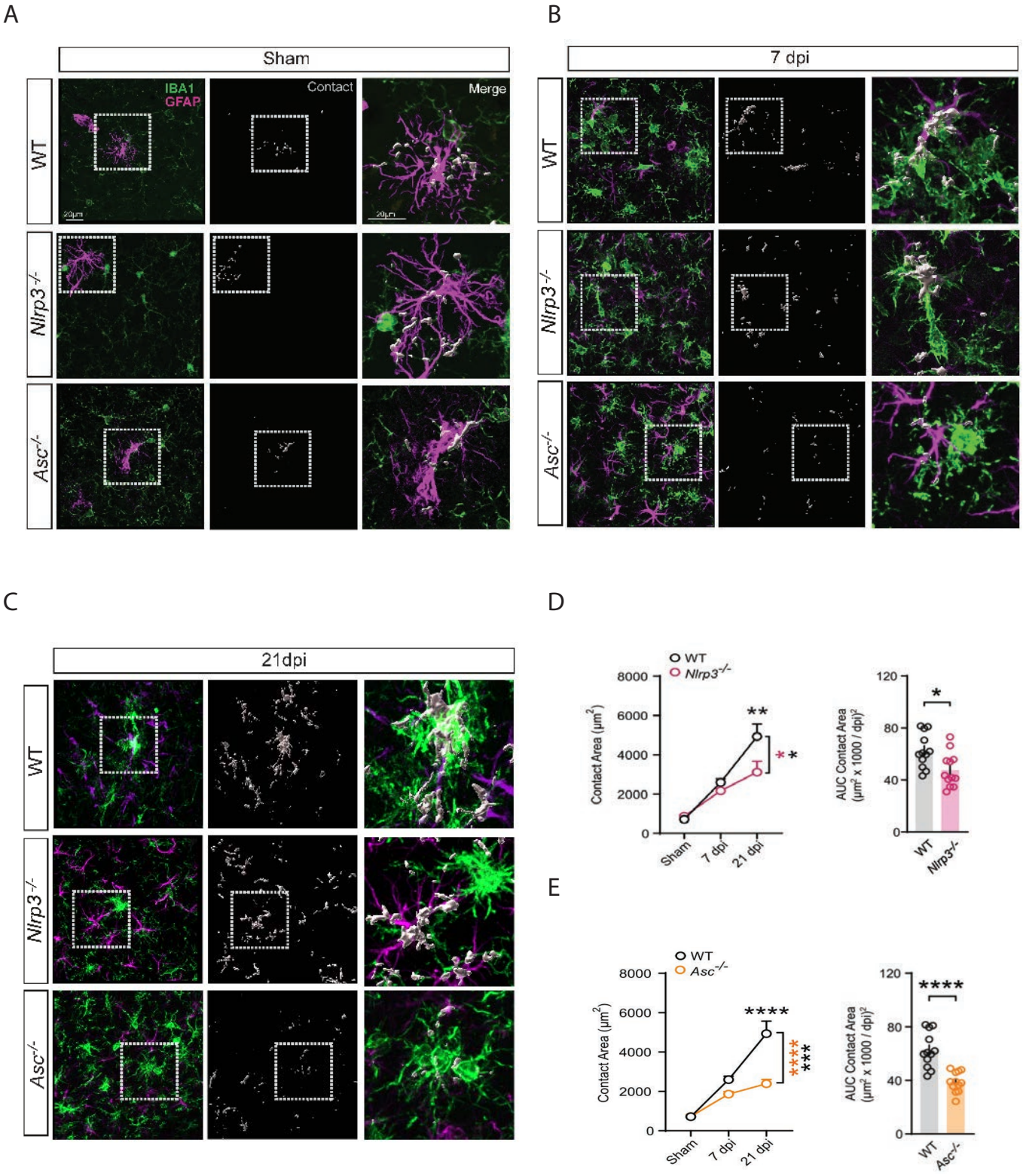
A
Sham
IBA1
GFAP
Contact
Merge
WT
Nlrp3-/-
Asc-/-
B
7 dpi
C
21dpi
D
WT
Nlrp3-/-
Contact Area (µm2)
8000
6000
4000
2000
0
Sham
7 dpi
21 dpi
**
**
AUC Contact Area (µm2 x 1000 / dpi)2
120
80
40
*
E
Asc-/-
****
***

3.6.2 Contact Between Glial Cells Is Correlated with ASC Distribution

To further investigate the relationship between glial cell contact and ASC expression, we conducted an analysis of the correlation between ASC distribution and glial contact area using IMARIS **(Fig. 9A-B)**. Interestingly, we observed a highly positive correlation between glial contact and the number of extracellular ASC spots *(r = 0.8588, slope = 0.02939, correlation p < 0.0001)*. In contrast, although the correlations of glial contact with the number of intracellular ASC spots *(r = 0.7248, slope = 0.06477, correlation p < 0.0001)* and the overall count of ASC spots *(r = 0.7086, slope = 0.01341, correlation p < 0.0001)* decreased, these correlations remained notably positive **(Fig. 9C-E)**. In summary, the results revealed that glial contact largely depends on ASC expression, especially the number of extracellular ASC spots.

Fig. 9: The contact between Iba1$^+$ cells and GFAP$^+$ cells is correlated with ASC distribution
A–B. Representative IMARIS images of immunohistochemical staining for Iba1 (green) and GFAP (magenta) in the peri-contusional cortexes of both WT and NLRP3 mice at 7 dpi and 21 dpi to analyze the correlation between ASC distribution and contact area. Scale bar = 20 µm. **C–E.** The data from IMARIS showed a strong correlation between ASC distribution and contact area *(n = 58 slice, p < 0.0001, r and p values were obtained following Spearman's correlation analysis).*

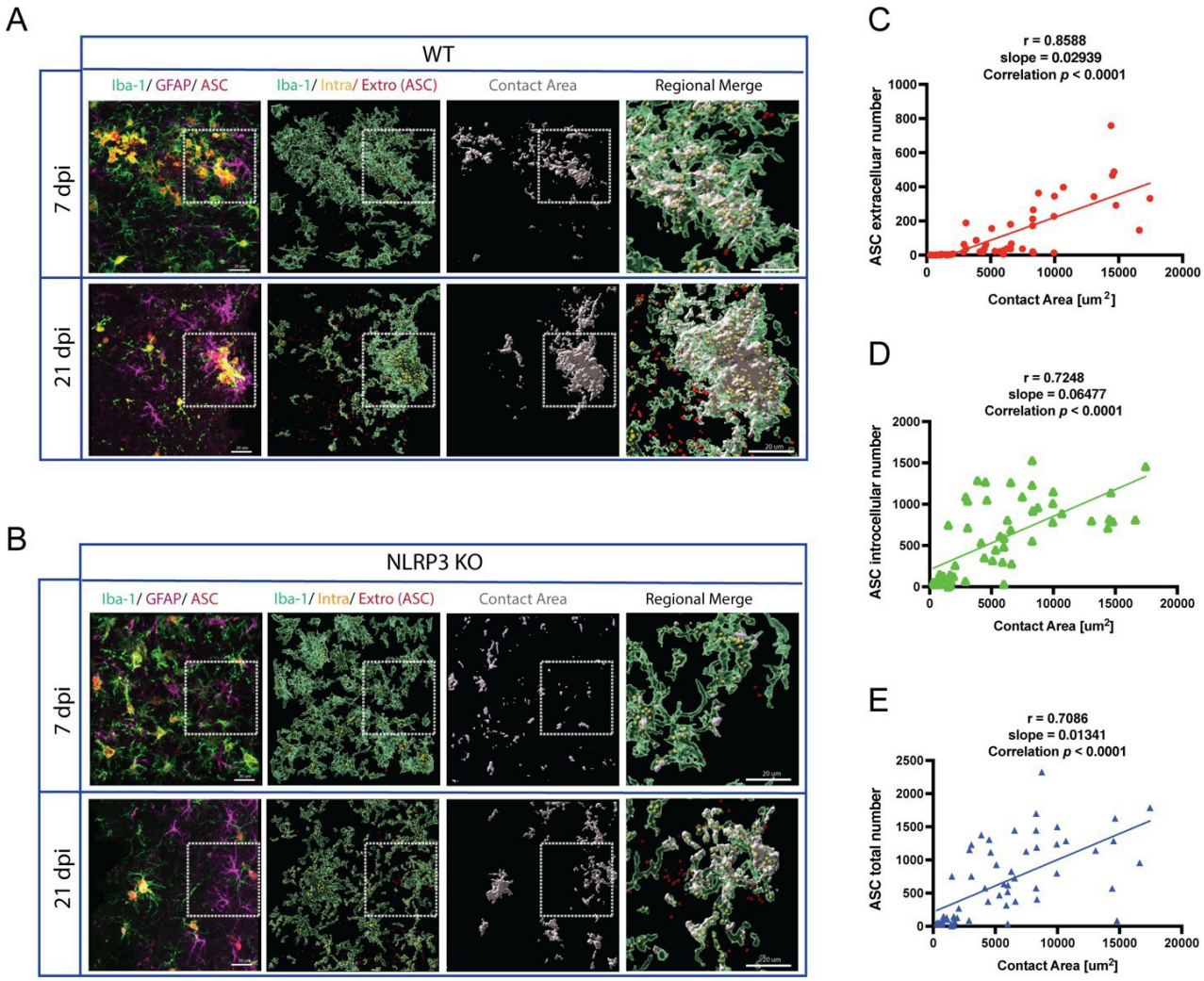

3.7 Potential types of microglial pyroptosis and their putative effects on astrocytes

3.7.1 Microglial Pyroptosis

We hypothesize that NLRP3 may be activated in microglia, leading to pyroptotic cell death. Within the framework of our injury model, a key observation has emerged: fused Iba1+ cells exhibited a significant increase in intracellular IL-1β expression and ASC aggregation, alongside the upregulation of extracellular ASC (Figure **10A-B**).

Based on this evidence, we propose that activation of the NLRP3 inflammasome occurs in these fused Iba1+ cells, inducing pyroptosis while simultaneously releasing pro-inflammatory factors and ASC.

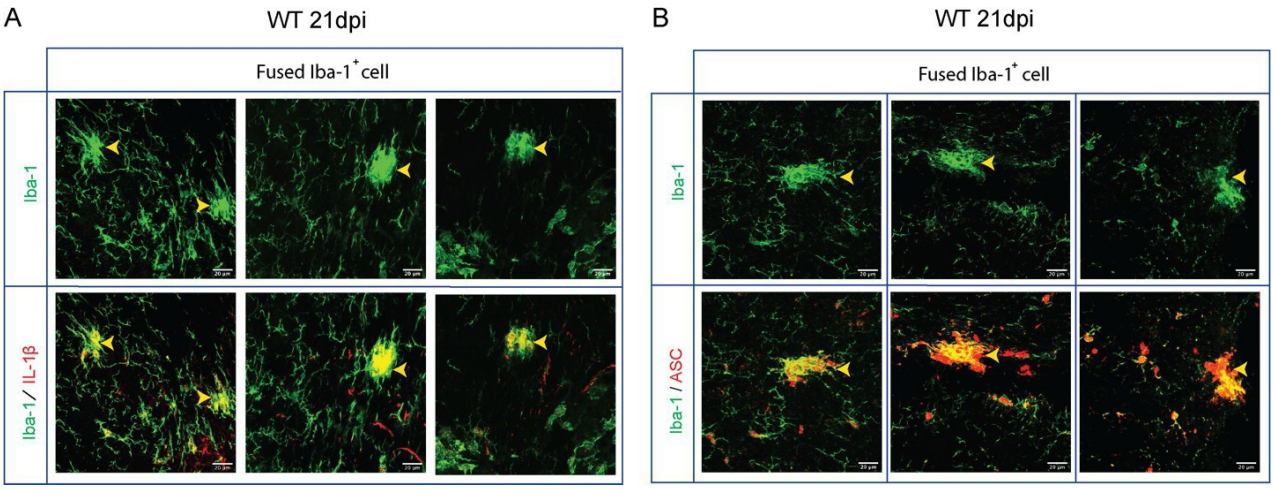

Fig. 10: Fused Iba1$^+$ cells show significant intracellular IL-1β expression and ASC aggregation
A-B. Representative image of immunohistochemical staining of the peri-contusional cortices of WT mice for Iba1 (green), IL-1β (red) or ASC (red) at 21dpi. Scale bar = 20 μm. White arrows emphasize fused Iba1$^+$ cells colocalized with IL-1β distinctly. Yellow arrows indicate fused Iba1$^+$ cells apparently colocalized with ASC, companied with massive extracellular ASC.

3.7.2 Putative Effects of Microglial Pyroptosis on astrocytes

To explore the potential effects of pyroptotic microglia on astrocytes, we observed that at 21 dpi, GFAP+ cells gathered around fused Iba1+ cells, but not around unfused cells. This aggregation led to the formation of a glial scar-like structure encapsulating the disintegrated Iba1+ cells and partially accumulated ASC (**Fig. 11D**). Interestingly, GFAP+ cell displayed notable ASC expression at 21 dpi, a feature absent at 7 dpi (**Fig. 11A-B**). Moreover, the contact volume between glial cells was greater at 21 dpi than at 7 dpi, suggesting a potential transfer of ASC from pyroptotic Iba1+ cells to astrocytes through direct contact (**Fig. 11C**).

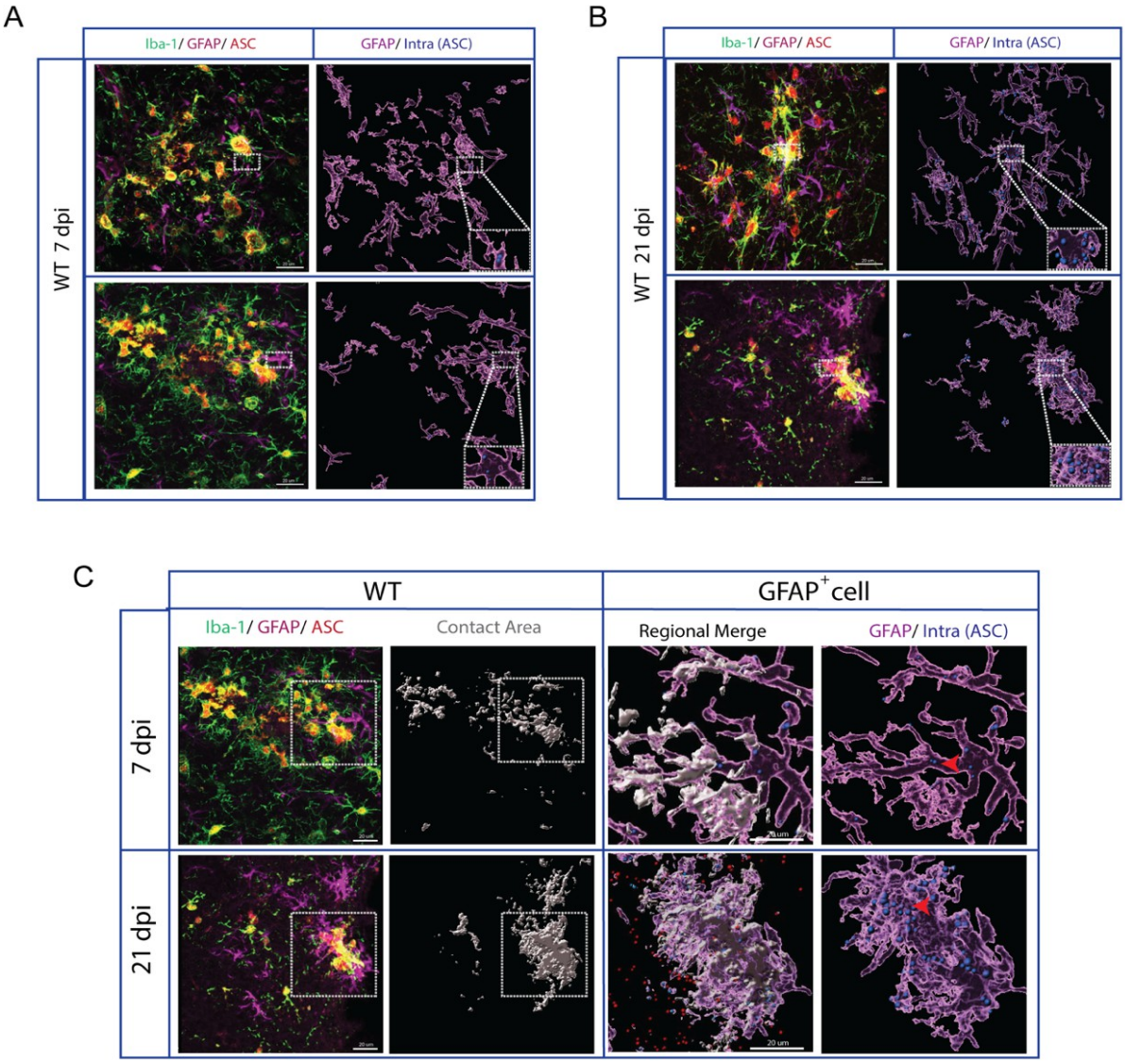
A
Iba-1/ GFAP/ ASC
GFAP/ Intra (ASC)
WT 7 dpi
B
Iba-1/ GFAP/ ASC
GFAP/ Intra (ASC)
WT 21 dpi
C
WT
GFAP+cell
Iba-1/ GFAP/ ASC
Contact Area
Regional Merge
GFAP/ Intra (ASC)
7 dpi
21 dpi
D
WT 21dpi
Unfused Iba-1+ cell
Fused Iba-1+ cell
Disintegrated Iba-1 +cell
Iba-1
Iba-1/ GFAP / ASC

Fig. 11: Glial interaction in the context of upregulation of ASC expression
A–D. Representative image of immunohistochemical staining of the peri-contusional cortices of WT mice for Iba1 (green), ASC (red), and GFAP (magenta) at 7 and 21 dpi. IMARIS analysis depicts Iba1$^+$ cell-originating ASC (yellow spheres), GFAP$^+$ cell-originating ASC (blue spheres), extracellular ASC (red spheres), and the contact area (gray). Scale bar = 20 µm. **A.** Sporadic and dispersed ASC specks were evident within astrocytes at 7 dpi. **B.** The abundance and volume of ASC within astrocytes increased at 21 dpi. **C.** As indicated by the red arrow, the GFAP$^+$ cells only expressed a few ASC after contacting with Iba-1$^+$ cells at 7 dpi. However, there was a significant increase in ASC expression in the contact area within GFAP$^+$ cells at 21 days post-injury. **D.** The yellow arrows indicate the interaction between fused Iba1$^+$ cells and hypertrophied GFAP$^+$ cells.

3.8 Upregulation of CASP-8 and CASP-3 Following mTBI

To investigate the potential apoptosis pathways influenced by TNF-α in our injury model, we conducted western blot analysis to assess the expression levels of cleaved CASP-8 and cleaved CASP-3 (**Fig. 12A–B**). We observed a significant increase in the expression levels of cleaved CASP-8 at 7 dpi, with a peak at 21 dpi *(Bonferroni's test, dpi F(3,24) ****p < 0.0001)* **(Fig. 12C–F**). Interestingly, the NLRP3 KO and ASC KO groups exhibited significantly reduced CASP-8 expression at 21 dpi compared with the WT group *(Bonferroni's test, WT 21 dpi vs. KO 21 dpi, ***p < 0.001, ****p < 0.0001)* (**Fig. 12C–D**). These findings are consistent with the expression of cleaved CASP-3 observed in the WT and KO group *(Bonferroni's test, dpi F(3,24) ****p < 0.0001. WT 21 dpi vs. KO 21 dpi, *p<0.05, ***p < 0.001);* however, the ASC KO group showed more significantly reduced expression of CASP-3 at 21 dpi, compared with NLRP3 group (**Fig. 12E–F**). Furthermore, we investigated the potential apoptosis pathway within the microglia or infiltrating macrophages by performing immunohistochemical staining for Iba1, cleaved CASP-3, and P53 in the contusional cortices of WT mice at 7 and 21 dpi (**Fig. 12G–H**). We observed the colocalization of CASP-3 with Iba1$^+$ cells at 7 and 21 dpi (**Fig. 12G**). Interestingly, we also observed P53 signals colocalized with Iba1$^+$ cells at 21 dpi (**Fig. 12H**). These results indicate that apoptosis may be upregulated within microglia or infiltrating macrophages in response to the increased expression of NLRP3 and ASC. Indeed, it is worth noting that CASP-8 and CASP-3 are not exclusively associated with apoptosis but also play roles in cell necroptosis or pyroptosis (K. W. Chen et al. 2019; Bertheloot, Latz, and Franklin 2021).

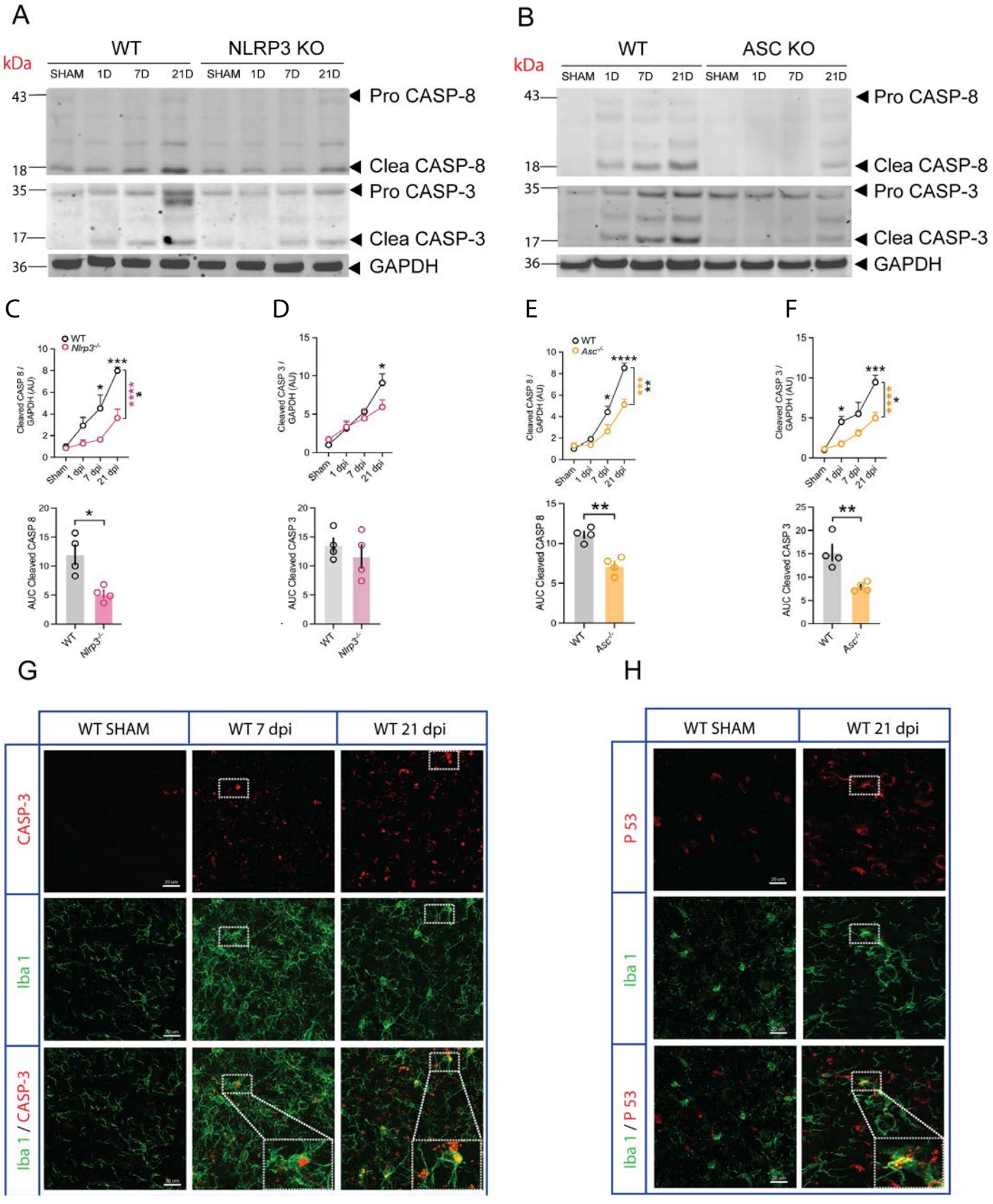
A
WT
NLRP3 KO
kDa
SHAM 1D 7D 21D SHAM 1D 7D 21D
43
18
35
17
36
Pro CASP-8
Clea CASP-8
Pro CASP-3
Clea CASP-3
GAPDH
B
WT
ASC KO
kDa
SHAM 1D 7D 21D SHAM 1D 7D 21D
43
18
35
17
36
Pro CASP-8
Clea CASP-8
Pro CASP-3
Clea CASP-3
GAPDH
C
WT
Nlrp3-/-
Cleaved CASP 8 / GAPDH (AU)
Sham 1 dpi 7 dpi 21 dpi
AUC Cleaved CASP 8
WT Nlrp3-/-
D
Cleaved CASP 3 / GAPDH (AU)
Sham 1 dpi 7 dpi 21 dpi
AUC Cleaved CASP 3
WT Nlrp3-/-
E
WT
Asc-/-
Cleaved CASP 8 / GAPDH (AU)
Sham 1 dpi 7 dpi 21 dpi
AUC Cleaved CASP 8
WT Asc-/-
F
Cleaved CASP 3 / GAPDH (AU)
Sham 1 dpi 7 dpi 21 dpi
AUC Cleaved CASP 3
WT Asc-/-
G
WT SHAM
WT 7 dpi
WT 21 dpi
CASP-3
Iba 1
Iba 1 / CASP-3
H
WT SHAM
WT 21 dpi
P 53
Iba 1
Iba 1 / P 53

Fig. 12: CASP-3 and CASP-8 expression increased significantly after injury
A–B Representative western blot images and densitometric semi-quantification of CASP-3 and CASP-8 in the peri-contusional cortices of mice subjected to surgery. **C–F.** The levels of cleaved CASP-8 and CASP-3 increased significantly at 7 dpi and peaked at 21 dpi compared with the SHAM group. Both NLRP3 KO and ASC KO decreased the expression of CASP-8 and CASP-3. **C-F.** ***Left panel:*** *Two-way ANOVA, Bonferroni's multiple comparisons test;* ***Right panel:*** *Two-tailed t-Tests represent integrated relative concentrations. AUC, Area Under Curve. n = 4 mice/group, *p < 0.05, **p < 0.01, ***p < 0.001, ****p < 0.0001. Data are presented as the mean ± SEM)*. **G–I**. Representative images of immunohistochemical staining for CASP-3, P53, and Iba1. Scale bar = 20 μm. **G.** CASP-3 (red) colocalized with $Iba1^+$ cells (green). **H.** P53 (red) colocalized with $Iba1^+$ cells (green) at 21 dpi.

4. Discussion

4.1 Temporal Profile of the NLRP3 Inflammasome and its Downstream Cytokines after mild Traumatic Brain Injury

In recent years, there has been growing interest in the role of NLRP3 in brain injuries, primarily because of its critical involvement in regulating the inflammatory cascade within the immune system. However, there is still a significant gap in our understanding of how NLRP3 contributes to sustained glial inflammation in cases of mTBI. In the present study, we comprehensively analyzed the expression patterns of NLRP3-associated proteins and a variety of downstream cytokines associated with NLRP3 following mTBI. Our study is among the first to investigate the NLRP3 expression profile up to 21 dpi in the context of mTBI. We observed increased expression levels of NLRP3, ASC, and pro-CASP-1 both at 7 and 21 dpi compared with the SHAM group. Additionally, dynamic changes in the protein levels of several downstream cytokines associated with NLRP3, including cleaved CASP-1, IL-1β, and TNF-a, were observed over time after mTBI. Their expression began to increase at 7 dpi and exhibited more pronounced upregulation at 21 dpi. However, it is important to note that numerous previous studies employing moderate-to-severe TBI models have consistently demonstrated that NLRP3 activation typically peaks within the initial 1–7 days following injury and subsequently declines over time. Ultimately, NLRP3-related protein levels return to baseline levels by 2 weeks post-injury (Dempsey et al., 2017; Liu et al., 2013; Xu et al., 2018). Contrary to these extensively reported TBI outcomes, our findings revealed a delayed activation of the NLRP3 inflammasome until 21 dpi as outlined above. This temporal pattern aligns with the findings of other researchers who have also observed a sustained inflammatory activation of microglia during the long-term phase (>21 dpi) following TBI (Jin et al., 2012b; Mouzon et al., 2014; Weil et al., 2014). These observations provide potential pathological evidence for delayed neurological symptoms in patients with mTBI.

4.2 Sustained Glial-Associated Inflammation Was Potentially Induced by NLRP3 Inflammasome Activation after mTBI

Numerous studies have consistently demonstrated the pivotal role of NLRP3 inflammasome activation within glial cells in regulating the intricate cascade of

neuroinflammatory processes (Dinarello, 2004; Heneka et al., 2013; Johann et al., 2015). Our investigation aligns with these findings, as we observed that both microglia and astrocytes exhibited notable pro-inflammatory characteristics 21 days after NLRP3 inflammasome activation. Intriguingly, our findings indicate that astrocytes contributed more to IL-1β expression than did microglia at 7 dpi, along with the earlier increase in the number of $GFAP^+$ cells at 1 dpi. Previous research has suggested that astrocytic proliferation and activation during the early phase of trauma can be induced by the STAT3 pathway, which facilitates tissue healing processes rather than deleterious effects (Wang et al., 2015; Zhao et al., 2011); And this regulated release of IL-1β can facilitate the clearance of damaged cells, thus promoting functional repair after trauma. In our study, the increased IL-1β induced primarily by astrocytes activation may account for the unimpaired R-NSS score at 7 dpi compared to the SHAM group (**Fig. 2D**). While, as the inflammatory milieu evolved toward 21 dpi, microglia emerged as the principal source of IL-1β release, far surpassing astrocytes. Similarly, several studies have demonstrated that microglia play a central role in driving sustained neurological injury beyond the subacute phase in TBI models (Todd et al., 2021; Witcher et al., 2018). Furthermore, our study highlights the significant role of NLRP3 in the aggregation of intracellular ASC and the upregulation of ASC outside the microglia at 21 dpi. These findings underscore the potential activation of the NLRP3 inflammasome in microglia and its role in regulating the glial-derived inflammatory cascade. Interestingly, it has been reported that microglia can further induce astrocyte inflammatory activity after NLRP3 inflammasome activation (Li et al., 2022). Moreover, it was reported that extracellular ASC can have prion-like properties and “infect” the neighboring glial cells, thereby triggering the activation of the ASC-mediated inflammasome cascade (Franklin et al., 2014; Friker et al., 2020; Venegas et al., 2017). These observations may explain why astrocytes exhibited more significant inflammatory activity at 21 dpi than at 7 dpi. Considering these findings, we speculate that the NLRP3 inflammasome plays an essential role in coordinating persistent glial inflammatory responses in cases of mTBI.

4.3 Contribution of NLRP3 to Glial Morphological Changes

It has been documented that glial cells can undergo adaptive functional changes and display temporal morphological alterations in response to inflammatory insults (Szabo and

Gulya, 2013 ; Savage et al ., 2019 ; Zhou et al ., 2019). Our study demonstrated that the morphologies of both microglia and astrocytes undergo de- ramification over time following brain injury. The most pronounced morphological changes, including signs of cell shrinkage, were observed at 21 dpi. Genetic removal of NLRP3 significantly alleviates these changes in glial cells. Furthermore, our investigations at 21 dpi revealed a notable presence of multinucleated giant $Iba1^+$ cells. This phenomenon is recognized as microglial clustering or microglial fusion, which is posited to play a pivotal role in expediting the clearance of debris and fostering immune responses. Nevertheless, an overabundance or unregulated clustering of microglial cells might potentially contribute to tissue harm and the onset of neuroinflammation (Zhong et al., 2019). Studies have also found that microglial fusion is closely related to the abnormal activation and degeneration of microglia, which are an integral part of the pathogenic cascade of diseases such as amyotrophic lateral sclerosis (Fendrick et al., 2007). We further hypothesize that these fused Iba1+ cells may represent a characteristic feature of pyroptosis following NLRP3 activation. These cells exhibited noticeable swelling, loss of normal cellular morphology, and a significant increase in both IL-1β expression and ASC aggregation (**Fig. 10A-B**).

4.4 NLRP3 Plays a Potential Role in Mediating the Interactions of Glial Cells

Numerous studies have emphasized that the morphological changes observed in microglia following TBI interact with the morphology of astrocytes (Morrison et al., 2017; Witcher et al., 2018). A previous study highlighted the connections between astrocytes and dysfunctional microglia, assuming that astrocytes play a compensatory role in phagocytosis of apoptotic cells (Konishi et al., 2020). In our current study, we observed active interactions between $GFAP^+$ and $Iba1^+$ cells through physical contact at both 7 and 21 dpi. Correlation analysis revealed a significant positive relationship between astrocyte–microglia contacts and the number of extracellular ASC spots. In previous studies, a potential connection has been identified between extracellular ASC and inflammatory signals, including IL-1β and TNF-α following inflammasome activation (Franklin et al., 2014). These cytokines could contribute to the aggregation of astrocytes around the activated microglia or infiltrating macrophages (Sofroniew, 2009; Wang et al., 2018a). This suggests that the astrocyte–microglia contacts may attribute to NLRP3 inflammasome activation induced ASC release after injury. Interestingly, a noticeable hypertrophy of

GFAP$^+$ cells at 21 dpi, rather than 7dpi, may be attributed to the potential trafficking of ASC from Iba1$^+$ cells (**Fig. 11A–C**). This mechanism may provide an explanation for the activation of astrocytes at 21 dpi in our study.

During the peak of inflammation, robust astrogliosis can synergize with microglia, in the formation of glial scars (Sofroniew, 2009; Wang et al., 2018a). Remarkably, at 21 dpi in our model, GFAP$^+$ cells clustered around the fused Iba1$^+$ cells but not the unfused cells. This resulted in the formation of a tissue that resembled a glial scar, encapsulating the disintegrated Iba1$^+$ cells and partially aggregating ASC **(Fig. 11D)**. The glial scar-like tissue might act as a physical and biochemical barrier to isolate the inflammatory cells, as reported in studies on glial scars (Tran et al., 2022; Zuidema et al., 2018). However, it is essential to note that a glial scar may be an important trigger for CNS injury to progress to neurodegenerative diseases (Ribotta et al., 2004; Silver and Miller, 2004; Wanner et al., 2008). These findings may underscore the role of microglial NLRP3 activation in promoting astrocytic aggregation through a pronounced inflammatory response, potentially influencing the formation of glial scars. Conclusively, our results suggest that glial morphological changes and their interaction in the context of NLRP3 activation can significantly influence post-brain injury processes.

4.5 Effect of NLRP3 Deficiency on Inflammation Process Following Injury

There is numerous research on the contribution of NLRP3 to post-TBI inflammation; however, many studies have reported conflicting results. Irrera et al. (2017) and Xu et al. (2018) demonstrated that NLRP3 KO mice subjected to injury exhibited reduced IL-1β and CASP-1 responses, suggesting a protective effect of NLRP3 deficiency on neuroinflammation and behavioral deficits within 7dpi (Irrera et al., 2017; Xu et al., 2018). However, Lopez- Rodriguez et al. did not observe any significant differences in mRNA expression of cytokines following NLRP3 KO compared to the WT group at 24h after TBI (Lopez- Rodriguez et al., 2022). This suggests that the impact of NLRP3 deficiency on neuroinflammation may vary depending on the specific experimental conditions or the different timepoint of analysis. In this study, we found decreased expression of inflammasome-related proteins and several pro-inflammatory cytokines in NLRP3 KO and ASC KO mice compared to WT mice at 21 dpi. Additionally, both groups of KO mice exhibited a rescue in the morphological changes of microglia and astrocytes after trauma

when compared to the SHAM group mice. For these two KO mice, ASC KO mice demonstrated a more pronounced effect in reducing the expression of cleaved CASP-1, IL-1β, and TNF-α than NLRP3 KO mice. These findings imply that while the NLRP3 pathway contributed significantly to the neuroinflammatory response in mTBI, it was likely not the sole determinant of the observed outcomes. Hence, other inflammatory pathways, cellular interactions, and signaling cascades may also play essential roles in the complex pathophysiology of TBI.

4.6 Interaction Between CASP-3 and NLRP3 Pathways

In recent years, the interplay between apoptotic and inflammasome pathways has attracted research attention (Bertheloot et al., 2021; Chen et al., 2019; Vince et al., 2018) (**Fig. 13**). Research has indicated that the apoptotic pathway can be triggered by the activation of TNF-related apoptosis-inducing ligand (TRAIL) and the BAX/BAK signaling pathway. CASP-3 serves a dual role in this context, acting as both an executor of apoptosis and participating in the activation of the NLRP3 pathway through potassium efflux (Chen et al., 2019; Vince et al., 2018). Notably, CASP-3 can cleave CASP-8, leading to the upregulation of cleaved IL-1β expression independently of the inflammasome activation (Vince et al., 2018). Conversely, the canonical activation of the NLRP3 inflammasome can induce the upregulation of TNF-α, subsequently initiating the TNF-α-related apoptotic pathway, which in turn promotes the expression of CASP-3 and CASP-8 (Chen et al. 2019; Xu et al. 2018).

In our study, we observed a significant increase in CASP-8 and CASP-3 levels at both 7 and 21 dpi, with a particularly notable increase at 21 dpi. Moreover, NLRP3 KO and ASC KO was associated with a decrease in CASP-8 expression, especially the ASC KO, which coincided with a declining trend in TNF-α levels. These findings suggest the possibility of TNF-α-related apoptosis involvement in our injury model. Notably, ASC knockout resulted in a more pronounced reduction in caspase-3 expression compared to NLRP3 knockout. This is in line with the involvements of ASC in both CASP-8 associated cell apoptosis and CASP-3 related cell necrosis reported in previous studies (Bertheloot et al. 2021 ; K. W. Chen et al. 2019; Motani et al. 2010), suggesting the preferential regulation of cell death by ASC after brain injury. Moreover, we also observed that cleaved CASP-3 and P53 co-localized with microglia at 21 dpi. Significantly, P53, a transcription factor that rapidly

responds to DNA damage, plays a key role in regulating the expression of several proapoptotic BCL-2 proteins (Walia et al ., 2011 ; Vaseva and Moll, 2009). This observation hints at the involvement of DNA damage-associated apoptosis in our model.

Interestingly, previously studies demonstrated that early induction of apoptosis may promote the downstream activation of NLRP3/caspase-1 and drive pyroptosis through the efflux of potassium. Additionally, apoptosis-induced potassium-activated ion channels have been reported to promote cell shrinkage or even cell death (Kunzelmann, 2016). This finding may underlie the significant shrinkage in microglia at 21 dpi and suggests a potential mechanism whereby the NLRP3 inflammasome in microglia at 21 dpi might be related to the efflux of potassium.

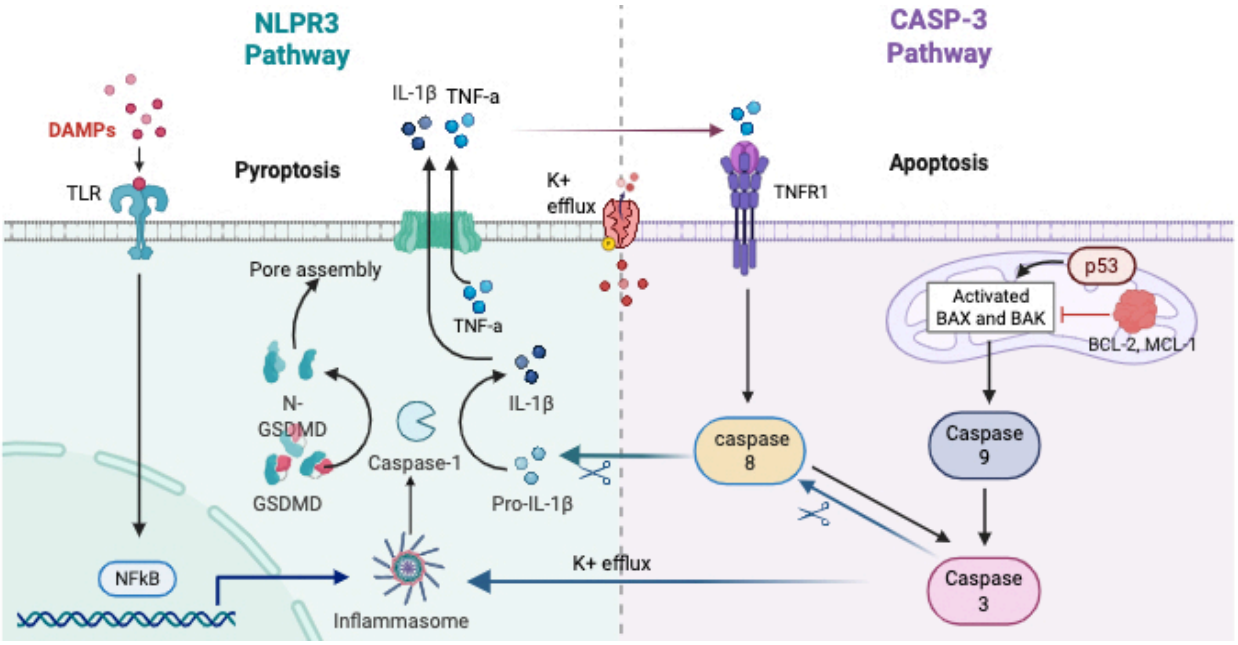

Fig. 13: Crosstalk between the NLRP3 and CASP-3 pathways
The canonical NLRP3 pathway promotes the expression of CASP-1-dependent IL-1β and the activation of TNF-α-associated apoptosis-dependent CASP-3. CASP-3 derived from BAX/BAK signaling and TNF-α-related apoptosis induces a parallel pathway of NLRP3 inflammasome-mediated CASP-1-dependent IL-1β maturation through potassium efflux. Simultaneously, it acts on CASP-8 upstream of the induced IL-1β maturation and secretion. Note: The figure was created using the Biorender website.

4.7 Other Inflammasomes Involved in Our mild Traumatic Brain Injury Model

The NLRP1, NLRP3, and AIM2 inflammasomes have been identified in microglia, astrocytes, and neurons following nervous system injury, contributing to neuroinflammatory responses, cell death, and exacerbated neurological outcomes (Freeman and Ting, 2016; Ge et al., 2018; de Rivero Vaccari et al., 2014). Importantly, different signals can induce the assembly of different inflammasomes. Inflammasome assembly involves interactions between the pyrin domain (PYD) or caspase activation and recruitment domain (CARD). Both PYD–PYD and CARD–CARD domains can oligomerize, serving as the foundation for inflammasome assembly. Significantly, the assembly of NLRP3 and AIM2 inflammasomes relies on the adapter ASC. In contrast, mouse NLRP1 can assemble pro-CASP-1 regardless of the presence of ASC (Guo et al., 2015; Van Opdenbosch et al., 2014) (**Fig. 14**). Activation of these inflammasomes results in cell pyroptosis, characterized by cell membrane rupture and the release of mature CASP-1 and IL-1β (de Rivero Vaccari et al., 2014). Interestingly, both NLRP3 and AIM2 inflammasomes share a common assembly mechanism mediated by the PYD domain for ASC polymerization. However, NLRP3 is more potent than AIM2 in promoting ASC polymerization during inflammasome formation (Lu et al., 2014).

In this study, we observed moderate ASC aggregation in NLRP3 KO mice, accompanied by a significant increase in extracellular ASC expression. These findings suggest the potential activation of AIM2 inflammasomes following mTBI. This may explain why the absence of ASC has a more apparent effect in terms of reducing the expression of CASP-1, -3, and -8, as well as reversing the morphology change than the absence of NLRP3. Moreover, previous studies have indicated that NLRP1-dependent neuronal pyroptosis plays a crucial role in cerebral hemorrhage or ischemia–reperfusion injury (Huang et al., 2021, Yan et al. 2021). Here, we revealed the expression of IL-1β in neurons at both 7 and 21 dpi in our study. This suggests that other ASC-independent inflammasomes, potentially NLRP1, may be activated in our injury model. Further investigations are required to establish a comprehensive understanding of inflammasome activation in the context of brain injury and its specific role in regulating inflammatory mediators.

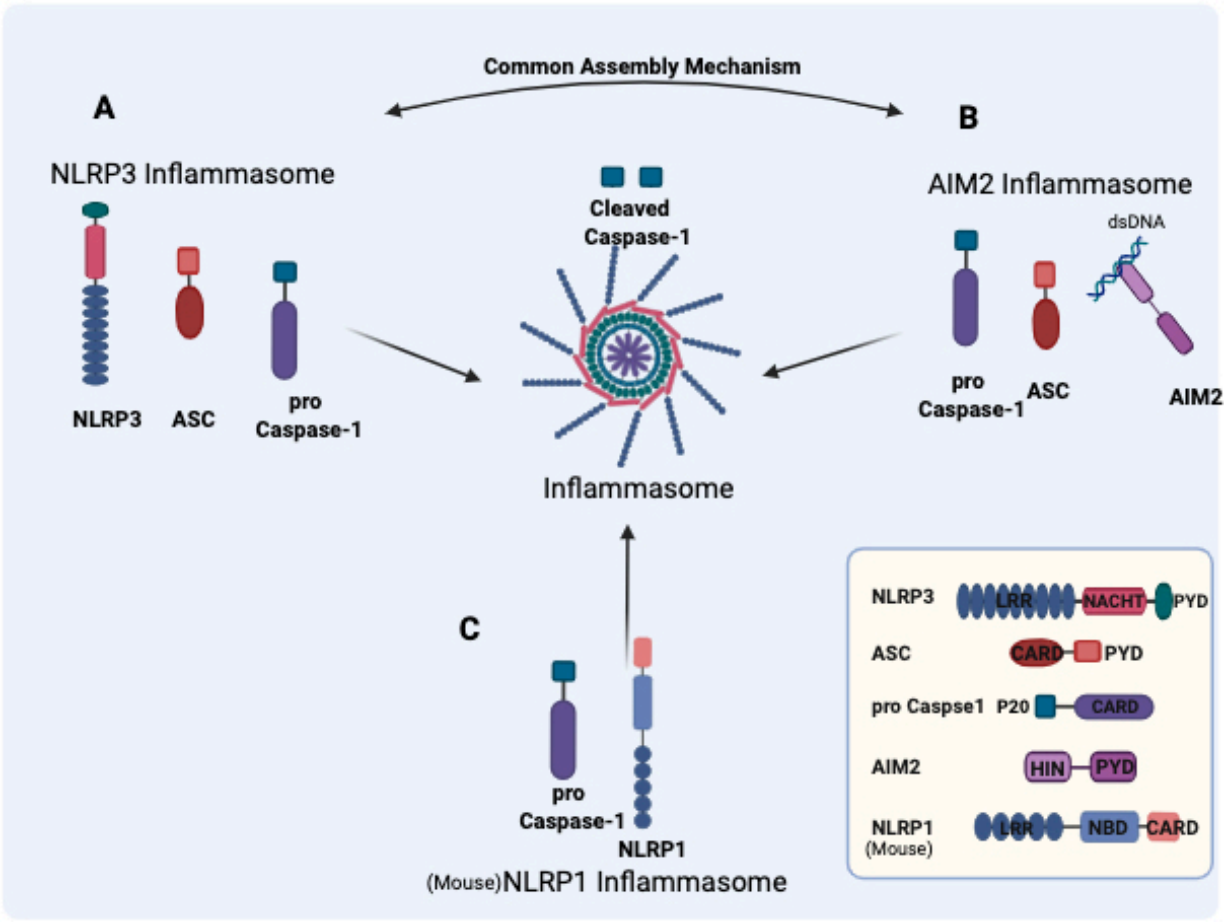

Fig. 14: Schematic assembly mechanism of NLRP3, AIM2, and NLRP1 inflammasomes **A.** The NLRP3 inflammasome comprises the NLRP3 protein, an ASC adaptor, and pro-CASP-1. Upon stimulation by DAMPs, NLRP3 undergoes structural changes in its leucine-rich repeat (LRR) domain, leading to its association with ASC via their PYD domains. ASC, in turn, associates with CASP-1 through its CARD domain. **B.** AIM2 inflammasomes share a common assembly mechanism with NLRP3 inflammasomes: The AIM2 protein can recognize and bind to double-stranded DNA (dsDNA) through its C-terminal HIN domains. Subsequently, it links with ASC and pro-CASP-1 to complete inflammasome assembly through interactions between their PYD and CARD domains.
C. Mouse NLRP1 can directly assemble pro-CASP-1 through homotypic interactions between the CARD domains for activation. After the inflammasome is assembled, multiple pro-CASP-1 molecules are recruited and undergo autocatalytic cleavage to produce p20 subunits. Note: The figure was created using the Biorender website.

4.8 Conclusion

The discussion above regarding the roles of microglia, astrocytes, and NLRP3 in neuroinflammation following mTBI provides valuable insights into their complex interactions. However, there are certain limitations that should be acknowledged. Our focus on NLRP3-ASC inflammasome-related proteins and glial morphological characteristics may not comprehensively capture the intricate dynamics of NLRP3 activation and other inflammatory mechanisms. Therefore, future research employing genomic, proteomic, and functional analyses at the single-cell level is necessary to gain a more profound understanding of the underlying mechanisms. Another limitation is the predominant focus on the post-traumatic neuroinflammatory responses of microglia and astrocytes, with less attention given to changes occurring in neurons and infiltrating cells. Besides, there is a need to investigate the inflammatory evolution of these neural and glial cells over a more extended post-traumatic period, in addition to assessing the activation status of NLRP3 and other ASC-related inflammasome.

Additionally, the interactions between microglia and astrocytes remain challenging to fully elucidate. Given the limited research on cell-cell contacts, the use of 3D processing technology, such as Imaris, for analyzing glial cell contacts remains underdeveloped and will require further refinement in future work. Regarding statistical methods, we primarily employed two-way repeated measures analysis of variance (ANOVA), which is well-suited for assessing interactions between injury time and gene type. However, this approach may introduce biases that could influence the interpretation and presentation of the results. Future studies should address these concerns by adopting more robust and diverse analytical techniques.

In light of the pathological mechanisms, pharmacological interventions targeting NLRP3, or ASC may help mitigate neuroinflammation, potentially promoting neuroprotection and enhancing recovery in CNS injury and degeneration. Future studies should delve into the specific pharmacological agents that can effectively modulate NLRP3 or ASC activity and assess their impact on neurological outcomes.

5. Summary

Traumatic Brain Injury is a significant global public health concern, particularly with the prevalence of mild traumatic brain injury. The neurological damage caused by mild traumatic brain injury is often heterogeneous, insidious, and persistent, yet our understanding of its fundamental pathophysiology remains limited. In this study, we hypothesized that the nucleotide-binding domain, leucine-rich-containing family, pyrin domain-containing-3 and apoptosis-associated speck-like protein containing a CARD inflammasome plays a crucial role in inducing glial inflammation and morphological responses following mild traumatic brain injury. This study employed a controlled skull impact–mild closed head injury model to delve into the molecular changes associated with mild traumatic brain injury. Notably, proteins linked to the nucleotide-binding domain, leucine-rich-containing family, pyrin domain-containing-3 inflammasome exhibited significant increases at both 7 and 21 days post-injury, coupled with elevated levels of cleaved caspase-1, interleukin-1 beta, and tumor necrosis factor-alpha, particularly prominent at 21 days post-injury. Immunohistochemical examinations unveiled interleukin-1 beta upregulation and apoptosis-associated speck-like protein containing a CARD aggregation within microglia, accompanied by a notable increase in extracellular ASC at 21 days post-injury. This may suggest that the nucleotide-binding domain, leucine- rich-containing family, pyrin domain-containing-3 inflammasome in microglia is predominantly activated at 21 days post-injury. Moreover, microglia exhibited distinct adaptive morphologies, including hypertrophy and shrinkage, forming giant cells at 21 days post-injury. Interestingly, morphological changes in astrocytes closely paralleled those in microglia. Astrocytes interacted with activated microglia under conditions of upregulated apoptosis-associated speck-like protein containing a CARD expression, associated with astrocyte hypertrophy and aggregation. This suggests that the apoptosis- associated speck-like protein containing a CARD pathway may contribute to glial interaction and impact the brain's reparative processes after mild traumatic brain injury. The study also predicts the involvement of the caspase-3 pathway and other apoptosis- associated speck-like protein containing a CARD-related inflammasomes in the injury model. The absence of nucleotide-binding domain, leucine-rich-containing family, pyrin domain-containing-3 and apoptosis-associated speck-like protein containing a CARD led to reduced levels of caspase-1 , caspase-3 , and caspase-8 , as well as downstream

cytokines, including interleukin-1 beta and tumor necrosis factor-alpha. Furthermore, nucleotide-binding domain, leucine-rich-containing family, pyrin domain- containing-3 and apoptosis-associated speck-like protein containing a CARD knockout mice exhibited attenuated morphological changes compared with wild-type mice. Notably, apoptosis-associated speck-like protein containing a CARD knockout appeared to have a more pronounced impact on reversing these pathological changes, indicating the involvement of other apoptosis-associated speck-like protein containing a CARD -related inflammasomes in the model. Overall, this study provides comprehensive insights into the molecular mechanisms, cellular interactions, and morphological changes associated with mild traumatic brain injury. The findings not only enhance our understanding of mild traumatic brain injury pathophysiology but also establish a solid foundation for future studies investigating pharmacological strategies targeting the nucleotide-binding domain, leucine-rich-containing family, pyrin domain-containing-3 -apoptosis-associated speck- like protein containing a CARD inflammasome.

6. List of figures

7. List of tables

8. References

Ahman S, Saveman B-I, Styrke J, Björnstig U, Stålnacke B-M. Long-term follow-up of patients with mild traumatic brain injury: a mixed-method study. J Rehabil Med 2013; 45: 758–764

Althammer F, Ferreira-Neto HC, Rubaharan M, Roy RK, Patel AA, Murphy A, Cox DN, Stern JE. Three-dimensional morphometric analysis reveals time-dependent structural changes in microglia and astrocytes in the central amygdala and hypothalamic paraventricular nucleus of heart failure rats. J Neuroinflammation 2020; 17: 221

Angelova DM, Brown DR. Microglia and the aging brain: are senescent microglia the key to neurodegeneration? J Neurochem 2019; 151: 676–688

Arganda-Carreras I, Fernández-González R, Muñoz-Barrutia A, Ortiz-De-Solorzano C. 3D reconstruction of histological sections: Application to mammary gland tissue. Microsc Res Tech 2010; 73: 1019–1029

Balasingam V, Tejada-Berges T, Wright E, Bouckova R, Yong VW. Reactive astrogliosis in the neonatal mouse brain and its modulation by cytokines. J Neurosci 1994; 14: 846– 856

Bertheloot D, Latz E, Franklin BS. Necroptosis, pyroptosis and apoptosis: an intricate game of cell death. Cell Mol Immunol 2021; 18: 1106–1121

Braun M, Vaibhav K, Saad NM, Fatima S, Vender JR, Baban B, Hoda MN, Dhandapani KM. White matter damage after traumatic brain injury: A role for damage associated molecular patterns. Biochim Biophys Acta Mol Basis Dis 2017; 1863: 2614–2626

Brett BL, Gardner RC, Godbout J, Dams-O'Connor K, Keene CD. Traumatic Brain Injury and Risk of Neurodegenerative Disorder. Biol Psychiatry 2022; 91: 498–507

Bryan NB, Dorfleutner A, Rojanasakul Y, Stehlik C. Activation of inflammasomes requires intracellular redistribution of the apoptotic speck-like protein containing a caspase recruitment domain. J Immunol 2009; 182: 3173–3182

Cassidy JD, Carroll LJ, Peloso PM, Borg J, von Holst H, Holm L, Kraus J, Coronado VG,

WHO Collaborating Centre Task Force on Mild Traumatic Brain Injury. Incidence, risk factors and prevention of mild traumatic brain injury: results of the WHO Collaborating Centre Task Force on Mild Traumatic Brain Injury. J Rehabil Med 2004; : 28–60

Chen H, Desai A, Kim H-Y. Repetitive Closed-Head Impact Model of Engineered Rotational Acceleration Induces Long-Term Cognitive Impairments with Persistent Astrogliosis and Microgliosis in Mice. J Neurotrauma 2017; 34: 2291–2302

Chen KW, Demarco B, Heilig R, Shkarina K, Boettcher A, Farady CJ, Pelczar P, Broz P. Extrinsic and intrinsic apoptosis activate pannexin-1 to drive NLRP3 inflammasome assembly. EMBO J 2019; 38: e101638

Clark E, Faruque S, Mutebi C, Nagirimadugu NV, Kim A, Mahendran M, Sullo E, Morey R, Turner RW. Investigating the relationship between mild traumatic brain injury and Alzheimer's disease and related dementias: a systematic review. J Neurol 2022; 269: 4635–4645

Crain JM, Nikodemova M, Watters JJ. Microglia express distinct M1 and M2 phenotypic markers in the postnatal and adult central nervous system in male and female mice. J Neurosci Res 2013; 91: 1143–1151

Davis BK, Wen H, Ting JP-Y. The inflammasome NLRs in immunity, inflammation, and associated diseases. Annu Rev Immunol 2011; 29: 707–735

Dejakaisaya H, Kwan P, Jones NC. Astrocyte and glutamate involvement in the pathogenesis of epilepsy in Alzheimer's disease. Epilepsia 2021; 62: 1485–1493

Dempsey C, Rubio Araiz A, Bryson KJ, Finucane O, Larkin C, Mills EL, Robertson A a. B, Cooper MA, O'Neill L a. J, Lynch MA. Inhibiting the NLRP3 inflammasome with MCC950 promotes non-phlogistic clearance of amyloid-β and cognitive function in APP/PS1 mice. Brain Behav Immun 2017; 61: 306–316

DePalma RG. Combat TBI: History, Epidemiology, and Injury Modes. In Brain Neurotrauma: Molecular, Neuropsychological, and Rehabilitation Aspects. FH Kobeissy (ed.). CRC Press/Taylor & Francis, Boca Raton (FL)

Dewan MC, Rattani A, Gupta S, Baticulon RE, Hung Y-C, Punchak M, Agrawal A, Adeleye AO, Shrime MG, Rubiano AM, Rosenfeld JV, Park KB. Estimating the global incidence of traumatic brain injury. J Neurosurg 2018; 130: 1080–1097

DiBona VL, Zhu W, Shah MK, Rafalia A, Ben Cheikh H, Crockett DP, Zhang H. Loss of Par1b/MARK2 primes microglia during brain development and enhances their sensitivity to injury. J Neuroinflammation 2019; 16: 11

Dinarello CA. Unraveling the NALP-3/IL-1beta inflammasome: a big lesson from a small mutation. Immunity 2004; 20: 243–244

Ebert SE, Jensen P, Ozenne B, Armand S, Svarer C, Stenbaek DS, Moeller K, Dyssegaard A, Thomsen G, Steinmetz J, Forchhammer BH, Knudsen GM, Pinborg LH. Molecular imaging of neuroinflammation in patients after mild traumatic brain injury: a longitudinal 123 I-CLINDE single photon emission computed tomography study. Eur J Neurol 2019; 26: 1426–1432

Fendrick SE, Xue Q-S, Streit WJ. Formation of multinucleated giant cells and microglial degeneration in rats expressing a mutant Cu/Zn superoxide dismutase gene. J Neuroinflammation 2007; 4: 9

Fenn AM, Gensel JC, Huang Y, Popovich PG, Lifshitz J, Godbout JP. Immune activation promotes depression 1 month after diffuse brain injury: a role for primed microglia. Biol Psychiatry 2014; 76: 575–584

Franchi L, Eigenbrod T, Muñoz-Planillo R, Nuñez G. The inflammasome: a caspase-1-activation platform that regulates immune responses and disease pathogenesis. Nat Immunol 2009; 10: 241–247

Franklin BS, Bossaller L, De Nardo D, Ratter JM, Stutz A, Engels G, Brenker C, Nordhoff M, Mirandola SR, Al-Amoudi A, Mangan MS, Zimmer S, Monks BG, Fricke M, Schmidt RE, Espevik T, Jones B, Jarnicki AG, Hansbro PM, Busto P, Marshak-Rothstein A, Hornemann S, Aguzzi A, Kastenmüller W, Latz E. The adaptor ASC has extracellular

and “prionoid” activities that propagate inflammation. Nat Immunol 2014; 15: 727–737
Freeman L, Guo H, David CN, Brickey WJ, Jha S, Ting JP-Y. NLR members NLRC4 and NLRP3 mediate sterile inflammasome activation in microglia and astrocytes. J Exp Med 2017; 214: 1351–1370

Freeman LC, Ting JP-Y. The pathogenic role of the inflammasome in neurodegenerative diseases. J Neurochem 2016; 136 Suppl 1: 29–38

Friker LL, Scheiblich H, Hochheiser IV, Brinkschulte R, Riedel D, Latz E, Geyer M, Heneka MT. β-Amyloid Clustering around ASC Fibrils Boosts Its Toxicity in Microglia. Cell Rep 2020; 30: 3743-3754.e6

Garaschuk O, Verkhratsky A. Physiology of Microglia. Methods Mol Biol 2019; 2034: 27–40

Gardner RC, Byers AL, Barnes DE, Li Y, Boscardin J, Yaffe K. Mild TBI and risk of Parkinson disease: A Chronic Effects of Neurotrauma Consortium Study. Neurology 2018; 90: e1771–e1779

Ge X, Li W, Huang S, Yin Z, Xu X, Chen F, Kong X, Wang H, Zhang J, Lei P. The pathological role of NLRs and AIM2 inflammasome-mediated pyroptosis in damaged blood-brain barrier after traumatic brain injury. Brain Res 2018; 1697: 10–20
Ghosh S, Castillo E, Frias ES, Swanson RA. Bioenergetic regulation of microglia. Glia 2018; 66: 1200–1212

Giulian D. Ameboid microglia as effectors of inflammation in the central nervous system. J Neurosci Res 1987; 18: 155–171, 132–133

Gombault A, Baron L, Couillin I. ATP release and purinergic signaling in NLRP3 inflammasome activation. Front Immunol 2012; 3: 414

González Ibanez F, Picard K, Bordeleau M, Sharma K, Bisht K, Tremblay M-È. Immunofluorescence Staining Using IBA1 and TMEM119 for Microglial Density, Morphology and Peripheral Myeloid Cell Infiltration Analysis in Mouse Brain. J Vis Exp

2019;

Gorgoulis V, Adams PD, Alimonti A, Bennett DC, Bischof O, Bishop C, Campisi J, Collado M, Evangelou K, Ferbeyre G, Gil J, Hara E, Krizhanovsky V, Jurk D, Maier AB, Narita M, Niedernhofer L, Passos JF, Robbins PD, Schmitt CA, Sedivy J, Vougas K, von Zglinicki T, Zhou D, Serrano M, Demaria M. Cellular Senescence: Defining a Path Forward. Cell 2019; 179: 813–827

Guo H, Callaway JB, Ting JP-Y. Inflammasomes: mechanism of action, role in disease, and therapeutics. Nat Med 2015; 21: 677–687

Guskiewicz KM, Broglio SP. Acute sports-related traumatic brain injury and repetitive concussion. Handb Clin Neurol 2015; 127: 157–172

Halle A, Hornung V, Petzold GC, Stewart CR, Monks BG, Reinheckel T, Fitzgerald KA, Latz E, Moore KJ, Golenbock DT. The NALP3 inflammasome is involved in the innate immune response to amyloid-beta. Nat Immunol 2008; 9: 857–865

Hart T, Novack TA, Temkin N, Barber J, Dikmen SS, Diaz-Arrastia R, Ricker J, Hesdorffer DC, Jallo J, Hsu NH, Zafonte R. Duration of Posttraumatic Amnesia Predicts Neuropsychological and Global Outcome in Complicated Mild Traumatic Brain Injury. J Head Trauma Rehabil 2016; 31: E1–E9

Hayashi K, Kadomatsu K, Muramatsu T. Requirement of chondroitin sulfate/dermatan sulfate recognition in midkine-dependent migration of macrophages. Glycoconj J 2001; 18: 401–406

Haynes SE, Hollopeter G, Yang G, Kurpius D, Dailey ME, Gan W-B, Julius D. The P2Y12 receptor regulates microglial activation by extracellular nucleotides. Nat Neurosci 2006; 9: 1512–1519

Heneka MT, Kummer MP, Stutz A, Delekate A, Schwartz S, Vieira-Saecker A, Griep A, Axt D, Remus A, Tzeng T-C, Gelpi E, Halle A, Korte M, Latz E, Golenbock DT. NLRP3 is activated in Alzheimer's disease and contributes to pathology in APP/PS1 mice. Nature 2013; 493: 674–678

Heneka MT, Kummer MP, Latz E. Innate immune activation in neurodegenerative disease. Nat Rev Immunol 2014; 14: 463–477

Hong S, Dissing-Olesen L, Stevens B. New insights on the role of microglia in synaptic pruning in health and disease. Curr Opin Neurobiol 2016; 36: 128–134

Huang L, Li X, Liu Y, Liang X, Ye H, Yang C, Hua L, Zhang X. Curcumin Alleviates Cerebral Ischemia-reperfusion Injury by Inhibiting NLRP1-dependent Neuronal Pyroptosis. Curr Neurovasc Res 2021; 18: 189–196

Irrera N, Pizzino G, Calò M, Pallio G, Mannino F, Famà F, Arcoraci V, Fodale V, David A, Francesca C, Minutoli L, Mazzon E, Bramanti P, Squadrito F, Altavilla D, Bitto A. Lack of the Nlrp3 Inflammasome Improves Mice Recovery Following Traumatic Brain Injury. Front Pharmacol 2017; 8: 459

Irrera N, Russo M, Pallio G, Bitto A, Mannino F, Minutoli L, Altavilla D, Squadrito F. The Role of NLRP3 Inflammasome in the Pathogenesis of Traumatic Brain Injury. IJMS 2020; 21: 6204

Ismael S, Nasoohi S, Ishrat T. MCC950, the Selective Inhibitor of Nucleotide Oligomerization Domain-Like Receptor Protein-3 Inflammasome, Protects Mice against Traumatic Brain Injury. J Neurotrauma 2018; 35: 1294–1303

Jassam YN, Izzy S, Whalen M, McGavern DB, El Khoury J. Neuroimmunology of Traumatic Brain Injury: Time for a Paradigm Shift. Neuron 2017; 95: 1246–1265

Jha MK, Jo M, Kim J-H, Suk K. Microglia-Astrocyte Crosstalk: An Intimate Molecular Conversation. Neuroscientist 2019; 25: 227–240

Jha S, Srivastava SY, Brickey WJ, Iocca H, Toews A, Morrison JP, Chen VS, Gris D, Matsushima GK, Ting JP-Y. The inflammasome sensor, NLRP3, regulates CNS inflammation and demyelination via caspase-1 and interleukin-18. J Neurosci 2010; 30: 15811–15820

Jin X, Ishii H, Bai Z, Itokazu T, Yamashita T. Temporal changes in cell marker expression

and cellular infiltration in a controlled cortical impact model in adult male C57BL/6 mice. PLoS One 2012a; 7: e41892

Jin X, Ishii H, Bai Z, Itokazu T, Yamashita T. Temporal changes in cell marker expression and cellular infiltration in a controlled cortical impact model in adult male C57BL/6 mice. PLoS One 2012b; 7: e41892

Johann S, Heitzer M, Kanagaratnam M, Goswami A, Rizo T, Weis J, Troost D, Beyer C. NLRP3 inflammasome is expressed by astrocytes in the SOD1 mouse model of ALS and in human sporadic ALS patients. Glia 2015; 63: 2260–2273

Johnson VE, Stewart W, Smith DH. Widespread τ and amyloid-β pathology many years after a single traumatic brain injury in humans. Brain Pathol 2012; 22: 142–149 Johnson VE, Stewart JE, Begbie FD, Trojanowski JQ, Smith DH, Stewart W. Inflammation and white matter degeneration persist for years after a single traumatic brain injury. Brain 2013; 136: 28–42

Kerr N, Lee SW, Perez-Barcena J, Crespi C, Ibañez J, Bullock MR, Dietrich WD, Keane RW, de Rivero Vaccari JP. Inflammasome proteins as biomarkers of traumatic brain injury. PLoS One 2018; 13: e0210128

Konishi H, Okamoto T, Hara Y, Komine O, Tamada H, Maeda M, Osako F, Kobayashi M, Nishiyama A, Kataoka Y, Takai T, Udagawa N, Jung S, Ozato K, Tamura T, Tsuda M, Yamanaka K, Ogi T, Sato K, Kiyama H. Astrocytic phagocytosis is a compensatory mechanism for microglial dysfunction. EMBO J 2020; 39: e104464

Kumar V. Toll-like receptors in the pathogenesis of neuroinflammation. J Neuroimmunol 2019; 332: 16–30

Kunzelmann K. Ion channels in regulated cell death. Cell Mol Life Sci 2016; 73: 2387–2403

Kuwar R, Rolfe A, Di L, Xu H, He L, Jiang Y, Zhang S, Sun D. A novel small molecular NLRP3 inflammasome inhibitor alleviates neuroinflammatory response following traumatic brain injury. J Neuroinflammation 2019; 16: 81

Leo P, McCrea M. Epidemiology. In Translational Research in Traumatic Brain Injury. D Laskowitz and G Grant (eds.). CRC Press/Taylor and Francis Group, Boca Raton (FL). Li B, Xia M, Zorec R, Parpura V, Verkhratsky A. Astrocytes in heavy metal neurotoxicity and neurodegeneration. Brain Res 2021a; 1752: 147234

Li L, Acioglu C, Heary RF, Elkabes S. Role of astroglial toll-like receptors (TLRs) in central nervous system infections, injury and neurodegenerative diseases. Brain Behav Immun 2021b; 91: 740–755

Li S, Fang Y, Zhang Y, Song M, Zhang X, Ding X, Yao H, Chen M, Sun Y, Ding J, Wang Q, Lu M, Wu G, Hu G. Microglial NLRP3 inflammasome activates neurotoxic astrocytes in depression-like mice. Cell Rep 2022; 41: 11153

Liddelow SA, Barres BA. Reactive Astrocytes: Production, Function, and Therapeutic Potential. Immunity 2017; 46: 957–967

Lin C, Chao H, Li Z, Xu X, Liu Y, Bao Z, Hou L, Liu Y, Wang X, You Y, Liu N, Ji J. Omega-3 fatty acids regulate NLRP3 inflammasome activation and prevent behavior deficits after traumatic brain injury. Exp Neurol 2017; 290: 115–122

Liu H-D, Li W, Chen Z-R, Hu Y-C, Zhang D-D, Shen W, Zhou M-L, Zhu L, Hang C-H. Expression of the NLRP3 inflammasome in cerebral cortex after traumatic brain injury in a rat model. Neurochem Res 2013; 38: 2072–2083

Liu X, Zhao Z, Ji R, Zhu J, Sui Q-Q, Knight GE, Burnstock G, He C, Yuan H, Xiang Z. Inhibition of P2X7 receptors improves outcomes after traumatic brain injury in rats. Purinergic Signal 2017; 13: 529–544

Loane DJ, Kumar A, Stoica BA, Cabatbat R, Faden AI. Progressive neurodegeneration after experimental brain trauma: association with chronic microglial activation. J Neuropathol Exp Neurol 2014; 73: 14–29

Lopez-Rodriguez AB, Decouty-Perez C, Farré-Alins V, Palomino-Antolín A, Narros-Fernández P, Egea J. Activation of NLRP3 Is Required for a Functional and Beneficial

Microglia Response after Brain Trauma. Pharmaceutics 2022; 14: 1550

Lu A, Magupalli VG, Ruan J, Yin Q, Atianand MK, Vos MR, Schröder GF, Fitzgerald KA, Wu H, Egelman EH. Unified polymerization mechanism for the assembly of ASC-dependent inflammasomes. Cell 2014; 156: 1193–1206

Lv W, Wang Z, Wu H, Zhang W, Xu J, Chen X. mTBI-Induced Systemic Vascular Dysfunction in a Mouse mTBI Model. Brain Sci 2022; 12: 232

Lynch JR, Wang H, Mace B, Leinenweber S, Warner DS, Bennett ER, Vitek MP, McKenna S, Laskowitz DT. A novel therapeutic derived from apolipoprotein E reduces brain inflammation and improves outcome after closed head injury. Exp Neurol 2005; 192: 109–116

McKee AC, Cantu RC, Nowinski CJ, Hedley-Whyte ET, Gavett BE, Budson AE, Santini VE, Lee H-S, Kubilus CA, Stern RA. Chronic traumatic encephalopathy in athletes: progressive tauopathy after repetitive head injury. J Neuropathol Exp Neurol 2009; 68: 709–735

Menon DK, Schwab K, Wright DW, Maas AI, Demographics and Clinical Assessment Working Group of the International and Interagency Initiative toward Common Data Elements for Research on Traumatic Brain Injury and Psychological Health. Position statement: definition of traumatic brain injury. Arch Phys Med Rehabil 2010; 91: 1637–1640

Morrison H, Young K, Qureshi M, Rowe RK, Lifshitz J. Quantitative microglia analyses reveal diverse morphologic responses in the rat cortex after diffuse brain injury. Sci Rep 2017; 7: 13211

Mouzon BC, Bachmeier C, Ferro A, Ojo J-O, Crynen G, Acker CM, Davies P, Mullan M, Stewart W, Crawford F. Chronic neuropathological and neurobehavioral changes in a repetitive mild traumatic brain injury model. Ann Neurol 2014; 75: 241–254

Muccigrosso MM, Ford J, Benner B, Moussa D, Burnsides C, Fenn AM, Popovich PG,

Lifshitz J, Walker FR, Eiferman DS, Godbout JP. Cognitive deficits develop 1month after diffuse brain injury and are exaggerated by microglia-associated reactivity to peripheral immune challenge. Brain Behav Immun 2016; 54: 95–109

Muñoz-Planillo R, Kuffa P, Martínez-Colón G, Smith BL, Rajendiran TM, Núñez G. K+ efflux is the common trigger of NLRP3 inflammasome activation by bacterial toxins and particulate matter. Immunity 2013; 38: 1142–1153

Norris JG, Tang LP, Sparacio SM, Benveniste EN. Signal transduction pathways mediating astrocyte IL-6 induction by IL-1 beta and tumor necrosis factor-alpha. J Immunol 1994; 152: 841–850

O'Brien WT, Pham L, Symons GF, Monif M, Shultz SR, McDonald SJ. The NLRP3 inflammasome in traumatic brain injury: potential as a biomarker and therapeutic target. J Neuroinflammation 2020a; 17: 104

O'Brien WT, Pham L, Symons GF, Monif M, Shultz SR, McDonald SJ. The NLRP3 inflammasome in traumatic brain injury: potential as a biomarker and therapeutic target. J Neuroinflammation 2020b; 17: 104

Orita H, Campeau JD, Gale JA, Nakamura RM, diZerega GS. Differential secretion of plasminogen activator activity by postsurgical activated macrophages. J Surg Res 1986; 41: 569–573

Paolicelli RC, Sierra A, Stevens B, Tremblay M-E, Aguzzi A, Ajami B, Amit I, Audinat E, Bechmann I, Bennett M, Bennett F, Bessis A, Biber K, Bilbo S, Blurton-Jones M, Boddeke E, Brites D, Brône B, Brown GC, Butovsky O, Carson MJ, Castellano B, Colonna M, Cowley SA, Cunningham C, Davalos D, De Jager PL, de Strooper B, Denes A, Eggen BJL, Eyo U, Galea E, Garel S, Ginhoux F, Glass CK, Gokce O, Gomez-Nicola D, González B, Gordon S, Graeber MB, Greenhalgh AD, Gressens P, Greter M, Gutmann DH, Haass C, Heneka MT, Heppner FL, Hong S, Hume DA, Jung S, Kettenmann H, Kipnis J, Koyama R, Lemke G, Lynch M, Majewska A, Malcangio M, Malm T, Mancuso R, Masuda T, Matteoli M, McColl BW, Miron VE, Molofsky AV, Monje M, Mracsko E, Nadjar A, Neher JJ, Neniskyte U, Neumann H, Noda M, Peng B, Peri F, Perry VH, Popovich PG, Pridans C,

Priller J, Prinz M, Ragozzino D, Ransohoff RM, Salter MW, Schaefer A, Schafer DP, Schwartz M, Simons M, Smith CJ, Streit WJ, Tay TL, Tsai L-H, Verkhratsky A, von Bernhardi R, Wake H, Wittamer V, Wolf SA, Wu L-J, Wyss-Coray T. Microglia states and nomenclature: A field at its crossroads. Neuron
2022; 110: 3458–3483

Perez-Polo JR, Rea HC, Johnson KM, Parsley MA, Unabia GC, Xu G, Infante SK, Dewitt DS, Hulsebosch CE. Inflammatory consequences in a rodent model of mild traumatic brain injury. J Neurotrauma 2013; 30: 727–740

Powell D, Stuart S, Godfrey A. Sports related concussion: an emerging era in digital sports technology. NPJ Digit Med 2021; 4: 164

Raj DDA, Jaarsma D, Holtman IR, Olah M, Ferreira FM, Schaafsma W, Brouwer N, Meijer MM, de Waard MC, van der Pluijm I, Brandt R, Kreft KL, Laman JD, de Haan G, Biber KPH, Hoeijmakers JHJ, Eggen BJL, Boddeke HWGM. Priming of microglia in a DNA-repair deficient model of accelerated aging. Neurobiol Aging 2014; 35: 2147–2160 Rathbone ATL, Tharmaradinam S, Jiang S, Rathbone MP, Kumbhare DA. A review of the neuro- and systemic inflammatory responses in post concussion symptoms: Introduction of the “post-inflammatory brain syndrome” PIBS. Brain Behav Immun 2015; 46: 1–16

Rhodes KE, Moon LDF, Fawcett JW. Inhibiting cell proliferation during formation of the glial scar: effects on axon regeneration in the CNS. Neuroscience 2003; 120: 41–56

Ribotta MG, Menet V, Privat A. Glial scar and axonal regeneration in the CNS: lessons from GFAP and vimentin transgenic mice. Acta Neurochir Suppl 2004; 89: 87–92

Ritzel RM, Doran SJ, Barrett JP, Henry RJ, Ma EL, Faden AI, Loane DJ. Chronic Alterations in Systemic Immune Function after Traumatic Brain Injury. J Neurotrauma 2018; 35: 1419–1436

Ritzel RM, Doran SJ, Glaser EP, Meadows VE, Faden AI, Stoica BA, Loane DJ. Old age increases microglial senescence, exacerbates secondary neuroinflammation, and worsens neurological outcomes after acute traumatic brain injury in mice. Neurobiol Aging 2019; 77: 194–206

de Rivero Vaccari JP, Dietrich WD, Keane RW. Activation and regulation of cellular inflammasomes: gaps in our knowledge for central nervous system injury. J Cereb Blood Flow Metab 2014; 34: 369–375

Robinson C, Apgar C, Shapiro LA. Astrocyte Hypertrophy Contributes to Aberrant Neurogenesis after Traumatic Brain Injury. Neural Plast 2016; 2016: 1347987

Rodríguez-Gómez JA, Kavanagh E, Engskog-Vlachos P, Engskog MKR, Herrera AJ, Espinosa-Oliva AM, Joseph B, Hajji N, Venero JL, Burguillos MA. Microglia: Agents of the CNS Pro-Inflammatory Response. Cells 2020; 9: 1717

Roth TL, Nayak D, Atanasijevic T, Koretsky AP, Latour LL, McGavern DB. Transcranial amelioration of inflammation and cell death after brain injury. Nature 2014; 505: 223– 228

Russo MV, McGavern DB. Immune Surveillance of the CNS following Infection and Injury. Trends Immunol 2015; 36: 637–650

Savage JC, Carrier M, Tremblay M-È. Morphology of Microglia Across Contexts of Health and Disease. Methods Mol Biol 2019; 2034: 13–26

Schlegelmilch T, Henke K, Peri F. Microglia in the developing brain: from immunity to behaviour. Curr Opin Neurobiol 2011; 21: 5–10

Schroder K, Tschopp J. The inflammasomes. Cell 2010; 140: 821–832

Shi J, Zhao Y, Wang K, Shi X, Wang Y, Huang H, Zhuang Y, Cai T, Wang F, Shao F. Cleavage of GSDMD by inflammatory caspases determines pyroptotic cell death. Nature 2015; 526: 660–665

Silver J, Miller JH. Regeneration beyond the glial scar. Nat Rev Neurosci 2004; 5: 146–156

Sofroniew MV. Molecular dissection of reactive astrogliosis and glial scar formation. Trends Neurosci 2009; 32: 638–647

Streit WJ, Braak H, Xue Q-S, Bechmann I. Dystrophic (senescent) rather than activated microglial cells are associated with tau pathology and likely precede neurodegeneration in

Alzheimer's disease. Acta Neuropathol 2009; 118: 475–485

Sun G, Miao Z, Ye Y, Zhao P, Fan L, Bao Z, Tu Y, Li C, Chao H, Xu X, Ji J. Curcumin alleviates neuroinflammation, enhances hippocampal neurogenesis, and improves spatial memory after traumatic brain injury. Brain Res Bull 2020; 162: 84–93

Susarla BTS, Villapol S, Yi J-H, Geller HM, Symes AJ. Temporal patterns of cortical proliferation of glial cell populations after traumatic brain injury in mice. ASN Neuro 2014; 6: 159–170

Sutterwala FS, Ogura Y, Szczepanik M, Lara-Tejero M, Lichtenberger GS, Grant EP, Bertin J, Coyle AJ, Galán JE, Askenase PW, Flavell RA. Critical role for NALP3/CIAS1/Cryopyrin in innate and adaptive immunity through its regulation of caspase-1. Immunity 2006; 24: 317–327

Swanson KV, Deng M, Ting JP-Y. The NLRP3 inflammasome: molecular activation and regulation to therapeutics. Nat Rev Immunol 2019; 19: 477–489

Szabo M, Gulya K. Development of the microglial phenotype in culture. Neuroscience 2013; 241: 280–295

Tam WY, Ma CHE. Bipolar/rod-shaped microglia are proliferating microglia with distinct M1/M2 phenotypes. Sci Rep 2014; 4: 7279

Taylor SE, Morganti-Kossmann C, Lifshitz J, Ziebell JM. Rod microglia: a morphological definition. PLoS One 2014; 9: e97096

Thelin EP, Carpenter KLH, Hutchinson PJ, Helmy A. Microdialysis Monitoring in Clinical Traumatic Brain Injury and Its Role in Neuroprotective Drug Development. AAPS J 2017; 19: 367–376

Todd BP, Chimenti MS, Luo Z, Ferguson PJ, Bassuk AG, Newell EA. Traumatic brain injury results in unique microglial and astrocyte transcriptomes enriched for type I interferon response. J Neuroinflammation 2021; 18: 151

Tran AP, Warren PM, Silver J. New insights into glial scar formation after spinal cord injury. Cell Tissue Res 2022; 387: 319–336

Vainchtein ID, Molofsky AV. Astrocytes and Microglia: In Sickness and in Health. Trends Neurosci 2020; 43: 144–154

Van Camp N, Lavisse S, Roost P, Gubinelli F, Hillmer A, Boutin H. TSPO imaging in animal models of brain diseases. Eur J Nucl Med Mol Imaging 2021; 49: 77–109

Van Opdenbosch N, Gurung P, Vande Walle L, Fossoul A, Kanneganti T-D, Lamkanfi M. Activation of the NLRP1b inflammasome independently of ASC-mediated caspase-1 autoproteolysis and speck formation. Nat Commun 2014; 5: 3209

Vaseva AV, Moll UM. The mitochondrial p53 pathway. Biochim Biophys Acta 2009; 1787: 414–420

Venegas C, Kumar S, Franklin BS, Dierkes T, Brinkschulte R, Tejera D, Vieira-Saecker A, Schwartz S, Santarelli F, Kummer MP, Griep A, Gelpi E, Beilharz M, Riedel D, Golenbock DT, Geyer M, Walter J, Latz E, Heneka MT. Microglia-derived ASC specks cross-seed amyloid-β in Alzheimer's disease. Nature 2017; 552: 355–361

Verkhratsky A, Ho MS, Parpura V. Evolution of Neuroglia. Adv Exp Med Biol 2019; 1175: 15–44

Vince JE, Wong WW-L, Gentle I, Lawlor KE, Allam R, O'Reilly L, Mason K, Gross O, Ma S, Guarda G, Anderton H, Castillo R, Häcker G, Silke J, Tschopp J. Inhibitor of apoptosis proteins limit RIP3 kinase-dependent interleukin-1 activation. Immunity 2012; 36: 215–227

Vince JE, De Nardo D, Gao W, Vince AJ, Hall C, McArthur K, Simpson D, Vijayaraj S, Lindqvist LM, Bouillet P, Rizzacasa MA, Man SM, Silke J, Masters SL, Lessene G, Huang DCS, Gray DHD, Kile BT, Shao F, Lawlor KE. The Mitochondrial Apoptotic Effectors BAX/BAK Activate Caspase-3 and -7 to Trigger NLRP3 Inflammasome and Caspase-8 Driven IL-1β Activation. Cell Rep 2018; 25: 2339-2353.e4

Walia V, Kakar S, Elble R. Micromanagement of the mitochondrial apoptotic pathway by p53. Front Biosci (Landmark Ed) 2011; 16: 749–758

Walker DG, Lue L-F. Immune phenotypes of microglia in human neurodegenerative disease: challenges to detecting microglial polarization in human brains. Alzheimers Res Ther 2015; 7: 56

Wallisch JS, Simon DW, Bayır H, Bell MJ, Kochanek PM, Clark RSB. Cerebrospinal Fluid NLRP3 is Increased After Severe Traumatic Brain Injury in Infants and Children. Neurocrit Care 2017; 27: 44–50

Wang H, Song G, Chuang H, Chiu C, Abdelmaksoud A, Ye Y, Zhao L. Portrait of glial scar in neurological diseases. Int J Immunopathol Pharmacol 2018a; 31: 2058738418801406

Wang J, Xu C, Zhang K, Shi J, Liu Z, Wang X, Guo M, Lv J, Ding X. Inhibition of ASC enhances the protective role of salvianolic acid A in traumatic brain injury via inhibition of inflammation and recovery of mitochondrial function. Folia Neuropathol 2021; 59: 50– 66

Wang KK, Yang Z, Zhu T, Shi Y, Rubenstein R, Tyndall JA, Manley GT. An update on diagnostic and prognostic biomarkers for traumatic brain injury. Expert Rev Mol Diagn 2018b; 18: 165–180

Wang T, Yuan W, Liu Y, Zhang Y, Wang Z, Zhou X, Ning G, Zhang L, Yao L, Feng S, Kong X. The role of the JAK-STAT pathway in neural stem cells, neural progenitor cells and reactive astrocytes after spinal cord injury. Biomed Rep 2015; 3: 141–146

Wang Y-F, Parpura V. Central Role of Maladapted Astrocytic Plasticity in Ischemic Brain Edema Formation. Front Cell Neurosci 2016; 10: 129

Wanner IB, Deik A, Torres M, Rosendahl A, Neary JT, Lemmon VP, Bixby JL. A new in vitro model of the glial scar inhibits axon growth. Glia 2008; 56: 1691–1709

Webster KM, Sun M, Crack P, O'Brien TJ, Shultz SR, Semple BD. Inflammation in epileptogenesis after traumatic brain injury. J Neuroinflammation 2017; 14: 10

Weil ZM, Gaier KR, Karelina K. Injury timing alters metabolic, inflammatory and functional outcomes following repeated mild traumatic brain injury. Neurobiol Dis 2014; 70: 108–116

Witcher KG, Bray CE, Dziabis JE, McKim DB, Benner BN, Rowe RK, Kokiko-Cochran ON, Popovich PG, Lifshitz J, Eiferman DS, Godbout JP. Traumatic brain injury-induced neuronal damage in the somatosensory cortex causes formation of rod-shaped microglia that promote astrogliosis and persistent neuroinflammation. Glia 2018; 66: 2719–2736

Wu L, Kalish BT, Finander B, Cao T, Jin G, Yahya T, Levy ES, Kukreja B, LaRovere ES, Chung JY, Lo EH, Brown-Whalen A, El Khoury J, Kaplan DL, Whalen MJ. Repetitive Mild Closed Head Injury in Adolescent Mice Is Associated with Impaired Proteostasis, Neuroinflammation, and Tauopathy. J Neurosci 2022; 42: 2418–24

Xu X, Yin D, Ren H, Gao W, Li F, Sun D, Wu Y, Zhou S, Lyu L, Yang M, Xiong J, Han L, Jiang R, Zhang J. Selective NLRP3 inflammasome inhibitor reduces neuroinflammation and improves long-term neurological outcomes in a murine model of traumatic brain injury. Neurobiology of Disease 2018; 117: 15–27

Yan J, Xu W, Lenahan C, Huang L, Wen J, Li G, Hu X, Zheng W, Zhang JH, Tang J. CCR5 Activation Promotes NLRP1-Dependent Neuronal Pyroptosis via CCR5/PKA/CREB Pathway After Intracerebral Hemorrhage. Stroke 2021; 52: 4021–4032

Yang S-T, Hsiao I-T, Hsieh C-J, Chiang Y-H, Yen T-C, Chiu W-T, Lin K-J, Hu C-J. Accumulation of amyloid in cognitive impairment after mild traumatic brain injury. J Neurol Sci 2015; 349: 99–104

Zamanian JL, Xu L, Foo LC, Nouri N, Zhou L, Giffard RG, Barres BA. Genomic analysis of reactive astrogliosis. J Neurosci 2012; 32: 6391–6410

Zeiler FA, Thelin EP, Czosnyka M, Hutchinson PJ, Menon DK, Helmy A. Cerebrospinal Fluid and Microdialysis Cytokines in Severe Traumatic Brain Injury: A Scoping Systematic Review. Front Neurol 2017; 8: 331

Zhao J, Zhang Y, Li G, Su X, Hang C. Activation of JAK2/STAT pathway in cerebral cortex

after experimental traumatic brain injury of rats. Neurosci Lett 2011; 498: 147– 152

Zhong L, Xu Y, Zhuo R, Wang T, Wang K, Huang R, Wang D, Gao Y, Zhu Y, Sheng X, Chen K, Wang N, Zhu L, Can D, Marten Y, Shinohara M, Liu C-C, Du D, Sun H, Wen L, Xu H, Bu G, Chen X-F. Soluble TREM2 ameliorates pathological phenotypes by modulating microglial functions in an Alzheimer's disease model. Nat Commun 2019; 10: 1365

Zhou B, Zuo Y-X, Jiang R-T. Astrocyte morphology: Diversity, plasticity, and role in neurological diseases. CNS Neurosci Ther 2019; 25: 665–673

Ziebell JM, Taylor SE, Cao T, Harrison JL, Lifshitz J. Rod microglia: elongation, alignment, and coupling to form trains across the somatosensory cortex after experimental diffuse brain injury. J Neuroinflammation 2012; 9: 247

Zuidema JM, Gilbert RJ, Gottipati MK. Biomaterial Approaches to Modulate Reactive Astroglial Response. Cells Tissues Organs 2018; 205: 372–395

9. Declaration of personal contribution

I am I hereby declare that I conducted the majority of the research work presented in this thesis independently. This includes the collection of mouse samples, execution of biochemical experiments, data collection, data analysis, and interpretation. No data or material included in this thesis was generated or processed by others, nor was any externally shared dataset used.

Prof. Heneka and Dr. Dr. Sergio Castro-Gomez supported me in the planning of the scientific experiments. All animals used in this study were operated by Dr. Dr. Sergio Castro-Gomez, with my assistance during these specific procedures.

This declaration accurately reflects the extent of my personal contribution to the research.

10. Acknowledgments

I am sincerely grateful to my supervisor, Prof. Dr. Micheal T. Heneka, for providing me with the invaluable opportunity to work in his esteemed research group and pursue my Medical Doctoral Degree at the German Center for Neurodegenerative Diseases and the Hospital of Bonn University. His unwavering support and guidance throughout my MD journey have been instrumental in shaping my academic and professional growth.

I extend my heartfelt thanks to Dr. Dr. Sergio Castro-Gómez, for his invaluable assistance and mentorship during my lab work and the writing of this thesis. His expertise and encouragement have been invaluable to me.

I would also like to express my gratitude to all the current and former members of the 'AG Heneka lab for their camaraderie, constant help, support, and valuable advice. It has been a pleasure collaborating with each one of you, and I am particularly thankful to Deniz and Kishore for their exceptional support.

To my family and friends, I am deeply appreciative of your unwavering love and support throughout this journey. Your encouragement has been my driving force, and I owe my accomplishments to your belief in me. Thank you all for being an essential part of my academic and personal journey.

11. List of publications

Parts of this thesis are based on the following publications:

Li T, Gomez S, Lucena P, Saecker A, Schwartz S, Deng Y, Ding Y, Stein V, Latz E, Heneka M. ASC contributes to sustained glial reactivity and mild cognitive impairment after closed-head injury. bioRxiv 2025. Jun 19. 660521. DOI: https://doi.org/10.1101/2025.06.19.660521.

Gomez S, Saecker A, Manco J, **Li T**, Kulińska I, Weiss F, Meissner F, Schwartz S, Stein V, Heneka M. NLRP3 inhibition maintains microglia architecture and enhances behavioral recovery after traumatic brain injury. bioRxiv 2025. Jun 25. 660521. DOI: https://doi.org/10.1101/2025.06.25.660862.

Other publications:

Deng Y, Liu T, Scifo E, **Li T**, Xie K, Taschler B, Morsy S, Schaaf K, Ehninger A, Bano D, Ehninger D. Analysis of the senescence-associated cell surfaceome reveals potential senotherapeutic targets. Aging Cell. 2024 Dec;23(12):e14312. DOI: https://doi.org/10.1111/acel.14312.

Deng Y, Kumar A, Xie K, Schaaf K, Scifo E, Morsy S, **Li T**, Ehninger A, Bano D, Ehninger D. Targeting senescent cells with NKG2D-CAR T cells. Cell Death Discov. 2024 May 4;10(1):217. DOI: https://doi.org/10.1038/s41420-024-01976-7.